

國立臺灣大學理學院物理學研究所



碩士論文

Department of Physics

College of Science

National Taiwan University

Master Thesis

於染劑參雜液晶中實現光控制二倍頻與其在超解析顯微鏡之
應用

Optical controllable second harmonic generation based on
dye-doped liquid crystal film and its application to super
resolution microscopy

陳冠杰

Kuan-Chieh Chen

指導教授：朱士維 博士

Advisor: Shi-Wei Chu, Ph.D.

中華民國 103 年 7 月

July, 2014

誌謝



在實驗室也待了三年多，如今這裡的生活也隨著這本論文完成而接近尾聲。

這些年來所受的點滴，實在難以在這邊三言兩語一一道盡。

首先，我當然得謝謝我的家人，尤其是我的父母，因為他們讓我在物質上無虞，可以有充分的精力面對種種的挑戰。就算有時我忙得沒日沒夜時也沒多說一句怨言。

能完成這篇論文，從我的指導老師—朱士維教授那收穫良多，除了在學術上耐心教導外，老師對於演講的嚴格要求，也是我碩班收穫之一。但對我而言，受用最大的還是如何規畫與調整計畫。除此之外，老師自由的風格也讓我有利用閒暇從事我有興趣的事物，使的碩班生活更加圓滿。

在實驗上，當然非常感謝趙治宇教授在樣本製備上的協助，此外也很謝謝他的學生—汪超然不厭其煩的教學。而和實驗室的夥伴們相處也自然是我一輩子難忘的回憶。像是冠宇學長除了是我實驗上的啟蒙導師外，更是實驗室的活百科，任何疑難雜症都難不倒他。東榆學長在言語上的砥礪以及細心的教學則是讓我在最短的時間融入實驗室。彥達學長淵博的知識伴我熬過無數的期中期末考和蒙古高原。美瑜學姊則是實驗室的開心果，不時犧牲自己帶給我們歡笑。柏輔學長和學侑學長更是我們 STED 組的中流砥柱。也很謝謝國仁在忙碌之餘，還幫我們處理各種瑣事，當你的女朋友一定很棒。由於李炫的幫助，讓我注意到更多演講細節。若不是庭英和哲維維護 fiber laser 得宜，這本論文也沒辦法產生了，祝你們武運昌隆。至於運儒雖然我們實驗上並沒有太多交集，不過謝謝你沒搶我的女朋友。最後，我也很感謝學弟妹，每次回答你們的問題，都讓我有更深的體悟，看著你

們的日漸成長，也給了我不能輸給你們的想法而更加努力。

在這裡，我也要謝謝生活裡的其他人，因為他們為我的生活帶來許許多多不同的元素。像是我的女朋友，感謝她讓我的記憶力和手寫能力還不至於完全退化。也很謝謝花系列，他們是我生活最佳的潤滑劑。此外像是取暖團和班聯團，讓我有磨練話術的機會。

由於篇幅的關係，還有許多人沒有提及，在此致上最誠摯的歉意和謝意。



中文摘要



不論電控制或是光控制二倍頻皆被應用於光通訊和光儲存技術上。相較於電控制二倍頻，光控制二倍頻不但有更高的準確性，同時在控制的圖樣上也有更多的自由度。然而過往光控制二倍頻的結果有著些許壞處，包括低開關對比、有限的開關次數和較長的反應時間。

在這篇論文中，我們提出於染劑參雜液晶中利用光致轉變達成光控制二倍頻。和之前的光控制二倍頻比起來，這個方法不但可以重複開關，還有 80% 的調製深度以及秒以下的反應時間。

此外我們也提出兩個可能的機制。包括 optical Fredericks 轉變和 nematic-isotropic 相轉變。經過實驗證實，後者比較可能為主要機制。由於二倍頻無法在 isotropic 相中產生。藉由此特性，二倍頻可以有效被抑制達到高開關對比。另一方面，因為液晶的分子特性，反應時間相較於之前的實驗大幅縮短。最後，因為液晶並沒有產生任何化學變化，所以這是個可重複開關的光控制二倍頻。

在論文的最後，我們也提出光控制二倍頻的新應用—超解析顯微術。Reversible saturable optical fluorescence transitions (RESOLFT) microscopy 雖然已是一個成熟的技術，但由於其建立在螢光的開關。所以不可避免的光漂白和有限的開關次數成為一個待解決的問題。由於二倍頻並不會有光漂白的問題，所以光控制二倍頻很有機會取代螢光作為超解析顯微術的核心機制。

關鍵字: 二倍頻; 液晶; 抑制; 光控制; 超解析顯微術

ABSTRACT



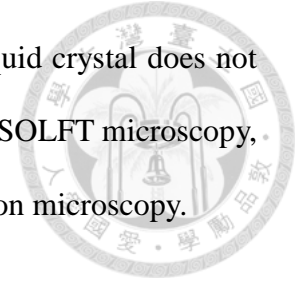
In the past, electrically or optically controllable second harmonic generation (SHG) has been applied to optical communication and storage. Compared with electrical control, optical one permits not only higher precision but also higher freedom in forming control pattern. However, previous methods of optically controllable SHG suffer from several drawbacks, including low on-off contrast, limited switch cycles and very long response time.

Here, we demonstrate a new idea of optically controllable SHG based on the light-induced transition of dye-doped liquid crystal (DDLIC) film. Compared with other optical methods, it is a reversible switch with 80-percent modulation depth and second-scale response time.

There are two possible mechanisms for this high-contrast, high-speed SHG switch, including optical Fredericks transition and nematic-isotropic phase transition. Based on transmittance, which is not altered by light, we have determined that nematic-isotropic phase transition is more likely the dominant mechanism. Because SHG is not allowed in isotropic phase and the dynamic motion of liquid crystal is much sooner than the materials, which were used in previous results, high-contrast and high-speed controllable SHG is realized. Besides, it is a reversible switch since chemical action is not involved in liquid crystal.

With the capability to optically switch on/off an optical signal, one novel application is superresolution microscopy. Reversible saturable optical fluorescence transitions (RESOLFT) microscopy, one of superresolution technics, is based on reversible switch of fluorescence. However, fluorescence suffers from photobleaching

and the limit of switching cycles. On the other hand, SHG from liquid crystal does not exhibit bleaching effect at all. Therefore, with similar scheme of RESOLFT microscopy, repeatable optically controllable SHG has potential in super resolution microscopy.



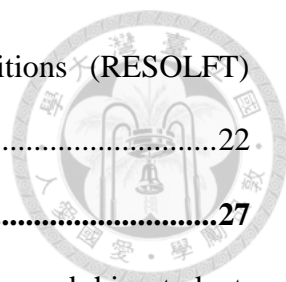
Keyword: second harmonic generation; liquid crystal; suppression; optically control; superresolution microscopy

CONTENTS



口試委員會審定書	#
誌謝	i
中文摘要	iii
ABSTRACT	iv
CONTENTS	vi
LIST OF FIGURES	viii
LIST OF TABLES	xi
Chapter 1 Introduction.....	1
Chapter 2 Theory	5
2.1 Second harmonic generation (SHG).....	5
2.1.1 Second order susceptibility	7
2.1.2 Noncentrosymmetric organization	9
2.1.3 Phase matching condition	9
2.1.4 SHG in nematic liquid crystal	11
2.2 Light-induced transition in dye-doped liquid crystal.....	13
2.2.1 Optical Fredericks transition	14
2.2.2 Nematic-isotropic phase transition.....	15
2.2.3 Potential of DDLC-based optically controllable SHG.....	16
2.3 Microscopic application.....	17
2.3.1 Confocal microscopy	17
2.3.2 Second harmonic generation (SHG) microscopy.....	20
2.3.3 Overview of superresolution microscopy	20

2.3.4	Reversible saturable optical fluorescence transitions (RESOLFT) microscope	22
Chapter 3	Sample and method.....	27
3.1	DDLC Sample (special thanks to Prof Chih-Yu Chao and his student, Chao-Ran Wang, for preparing sample)	27
3.1.1	Fine structure.....	28
3.2	Polarized light microscope	32
3.3	RESOLFT-like SHG microscopy	33
3.3.1	Setup.....	33
3.3.2	Time-correlated single photon counting (TCSPC).....	35
Chapter 4	Results and discussion	39
4.1	SHG in DDLC	39
4.2	Switchable and repeatable SHG	40
4.3	Mechanism of controllable SHG in DDLC	42
4.4	Response time of phase transition	44
4.5	Comparison with other optical controllable SHG	45
4.6	RESOLFT-like SHG microscopy	46
4.6.1	Nano-gold-doped sample	47
4.6.2	Artificial structure made by photoresist	47
Chapter 5	Conclusion	50
	REFERENCE	51



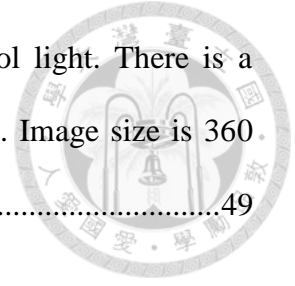
LIST OF FIGURES



Fig. 2.1	state diagram of SHG.....	5
Fig. 2.2	refractive index ellipsoid in the uniaxial medium	10
Fig. 2.3	The efficiency of SHG highly depends on the wavelength, polarization and orientation.	11
Fig. 2.4	the relationship between intensity of SHG and incident angle [37].	12
Fig. 2.5	Reversible optical switch between <i>trans</i> - and <i>cis</i> -azo-dye [22]	13
Fig. 2.6	Phase transition of DDLC. N, nematic; I, isotropic[28]. T_{ct} and T_{cc} are the nematic-isotropic phase transition temperature of the mixture with the <i>trans</i> - and <i>cis</i> form	16
Fig. 2.7	Scheme of confocal microscope [40]	18
Fig. 2.8	Airy disk	19
Fig. 2.9	The concept of STED. (a) Energy diagram, (b) depletion curve and (c) Setup of STED [47, 48]	22
Fig. 2.10	parabolic approximation of depletion beam [49].....	23
Fig. 2.11	the relationship between effective PSF and $\zeta(\equiv \frac{I_{Dep}}{I_{sat}})$ [47].....	25
Fig. 2.12	Photobleaching demonstration on actin of melanin cell stained by Alexa-488 ($I \cong 10^7 W/cm^2$).....	25
Fig. 3.1	structural formula and spectra [52] of DR1	27
Fig. 3.2	Sectional drawing of nano-gold-doped sample	29
Fig. 3.3	The glass coated with photoresist and the cross-sectional drawing of cell ..	31
Fig. 3.4	Polarized light microscope setup	33

Fig. 3.5	Setup	34
Fig. 3.6	Scheme of synchronizing scanning stage and TCSPC system	35
Fig. 3.7	Detector signal for fluorescence detection at a pulse repetition rate of 80 MHz	36
Fig. 3.8	Relationship between reference and detector signal.....	37
Fig. 3.9	Principle of reconstructing waveform	37
Fig. 3.10	Distinguish SHG signal from fluorescence	38
Fig. 4.1	SHG intensity is dependent on direction of polarization.....	39
Fig. 4.2	SHG is depleted by control light, 473-nm CW laser	41
Fig. 4.3	Intensity distribution of PSFs in lateral direction. Red, green and blue curve mean normalized intensity distribution of excitation light, SHG and control light respectively.....	41
Fig. 4.4	Switchable and reversible optical controllable SHG.....	42
Fig. 4.5	The relationship between directions of two PBS and sample.....	44
Fig. 4.6	Transmittance of probe light is changed by control light	45
Fig. 4.7	SHG image of usual DDLC sample with (a) near-infrared laser only. (b) both near-infrared laser and doughnut-shaped control light. Both image sizes are $10\ \mu\text{m} \times 10\ \mu\text{m}$	46
Fig. 4.8	Backward scattering image of nano-gold-doped DDLC sample (a) before (b) after illuminated by 473-nm laser. Both image sizes are $10\ \mu\text{m} \times 10\ \mu\text{m}$	47
Fig. 4.9	(a) Backward scattering image and (b) SHG image of artificial structure. Arrows point out the edge of hole. Both image sizes are $13.8\ \mu\text{m} \times 13.8\ \mu\text{m}$. (c) Line profile of SHG image. The FWHM of the peak is about $1.3\ \mu\text{m}$, which is much larger than the PSF. It means it could not be used to determine the resolution.	48

Fig. 4.10 Image of artificial structure after illuminated by control light. There is a obvious defect in the edge of hole due to photodamage. Image size is 360. $\mu\text{m} \times 360 \mu\text{m}$49



LIST OF TABLES



Table 4.1 Result of polarized light microscope for the study of mechanism43

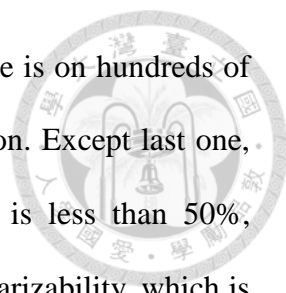
Chapter 1 Introduction



Under low light intensity, the relationship between light and matter is a linear interaction. It means the polarization of molecules is proportional to the incident electric field. Compared with nonlinear elasticity, one of nonlinear effects, a strong stress is required in order to induce nonlinear strain. Similarly, an intense light source is required for triggering nonlinear optics (NLO) effects. Therefore, in 1960s, NLO, which is including second harmonic generation (SHG) [1], multi-photon fluorescence [2, 3], third harmonic generation [4] and so on, was demonstrated right after the invention of ruby laser, which provides enough intensity [5]. Up to present, NLO has great amount of applications in various fields, including biological imaging [6, 7], communication [8], laser [9, 10] and others.

SHG, as one of the most well-known and first-demonstrated NLO effects, is highly dependent on the geometry of molecules. Thus, SHG can be used to detect the structure and orientation of molecule [11]. With the capability to control molecular structure or orientation, both electrical [12-14] and optical methods [15-19] establish controllable SHG, which is applied to optical communication [13, 17] and storage [20, 21]. The former methods have advantage of short response time and high contrast. Nevertheless, optical one permits not only higher precision but also higher freedom in forming control pattern.

The optically controllable SHG has been previously demonstrated in poled polymers containing photochromic dyes [15, 16], organic photochromic crystals [17, 18] and two-photon isomerization of azobenzene moieties in cross-linked



ferroelectric liquid-crystalline polymers[19]. The response time is on hundreds of second scale due to the response time of photochromic reaction. Except last one, all of these results suffer from low on-off contrast, which is less than 50%, because they are based on modification of molecular hyperpolarizability, which is hard to be modulated to zero. Besides, controllable SHG in poled polymers faces the problem of irreversible changes in the initial chromophore alignment after several switches. It limits the number of on-off cycles of SHG. Therefore, a high-contrast, high-speed and reversible optical controllable SHG is worthy to be studied.

In this thesis, we present a new scheme of controllable SHG, which is based on light-induced transition in dye-doped liquid crystal (DDLIC). DDLIC is liquid crystal mixed with a small amount of azo dye. Liquid crystal is one of the most well-known soft materials around the world. It is used in display devices because it can be easily controlled by electrical or optical field and sub-second response time.

It is notable that azo dye has been studied for a long time because this rod-like molecule has been also reported has photochemical *trans* \leftrightarrow *cis* isomerization induced by UV or visible light [22-24]. In the following two paragraphs, possible mechanisms of optically controllable SHG are discussed. In this thesis, figuring out the mechanism of controllable SHG is one of our aims.

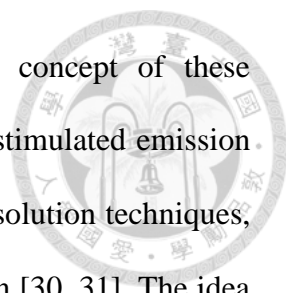
In 1990, Janossy has found that, by dissolving a small amount of azo dye, the orientation of liquid crystal trend to be perpendicular to polarization of incident beam [25, 26]. Moreover, the optical Fredericks transition (OFT) threshold is reduced by two orders of magnitude in contrast to pure liquid crystal cell [27]. Because the efficiency of SHG highly depends on the angle between the

orientation of liquid crystal and the polarization of incident light, it is possible to control SHG by dye-enhanced OFT.

On the other hand, due to phase matching condition, SHG should not be generated in noncentrosymmetric material, such as isotropic phase. In other words, controllable SHG can be demonstrated by phase transition. In DDLC, the nematic-isotropic phase transition temperature is also changed. It is because *trans* form isomer of azo dye is rod-like shape, which is similar to the structure of nematic liquid crystal while the *cis*-form is bent. It causes the *trans* one stabilizes phase structure in liquid crystal phase. Oppositely, the latter one destabilizes the phase structure of the mixture. As a result, the nematic-isotropic phase transition temperature of liquid crystal with *cis* form is lower than that with *trans* form [28].

Due to the dynamics of liquid crystal, the response time have potential in second scale or less. Moreover, instead of modulation of hyperpolarizability, molecular dynamics is considered in both possible mechanisms. Therefore, the contrast could be higher than previous results. Because there is no chemical reaction in liquid crystal, SHG should not decrease after several switch cycles. To sum up, DDLC might be a suitable sample for controllable SHG because it has advantage over previous results in terms of response time, contrast and reversibility.

In the last part of this thesis, we propose a new idea of superresolution microscopy based on this optical controllable SHG. Traditional optical microscopy is widely used to examine biological specimens because it provides a real-time, non-invasive and 3-dimensional observation. However, conventional optical microscopy is limited by relatively low spatial resolution due to diffraction of light. Thus, to overcome diffraction barrier, a number of superresolution



microscopy techniques have been invented [29, 30]. The concept of these superresolution methods is nonlinear responses. For example, stimulated emission depletion (STED) microscopy, one of most successful superresolution techniques, is based on the nonlinear response of fluorophores to excitation [30, 31]. The idea is combining two light. One is excitation. The other one is depletion light. First one is used to excite fluorophores from ground state to excited state, while the other one depletes the fluorophores in excited state via stimulated emission. To turn off the fluorescence in the peripheral focal spot, a vortex phase plate phase, which converts depletion light to doughnut-shape, is necessary. Therefore, with proper filter, the effective focal spot is smaller. However, to achieve superresolution, it requires intense depletion light, which causes photobleaching. The basic idea of STED is switchable and repeatable. In other words, not only fluorescence but also any signal with these two properties has potential to demonstrate superresolution [32, 33]. Thus, non-bleaching method becomes a new challenge of superresolution techniques.

Because optical controllable SHG exhibits both switchable and repeatable property, superresolution based on it deserves to attempt. Because the mechanism is not fluorescence, it does not suffer from photobleaching. Besides, due to optical section, SHG microscopy also provides good axial resolution without the need of pinhole, which is required in confocal microscopy and decrease the intensity of signal.

Chapter 2 Theory



2.1 Second harmonic generation (SHG)

Generally, polarization is linear to the incident electric field. However, if optical field is strong enough, nonlinearity is revealed. One of most famous nonlinear optics is SHG. From Fig. 2.1, two identical photons interact with material and unify into a new one. Due to conservation of energy, the frequency of new photon is twice than original frequency.

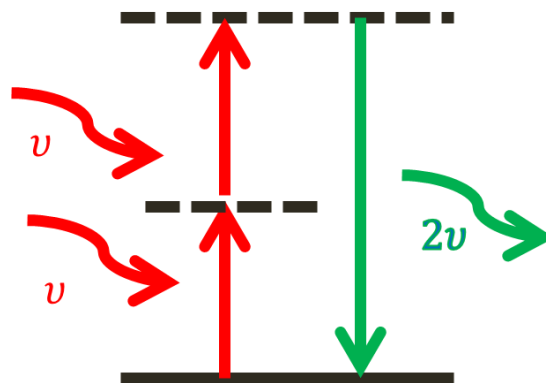


Fig. 2.1 state diagram of SHG

For detailed explanation of SHG, quantum physics is necessary. However, due to the Lorentz's effort, SHG can be described by forced harmonic oscillator model. In this model, electrons are considered as an oscillator driven by external electric field. Molecule is polarized by applied field and dipole moment p is defined by

$$p = -qx \quad (2.1)$$

Where q is electric charge of electron, x is field induced displacement. The bulk polarization P is given by

$$P = -Np \quad (2.2)$$

Where N is the electron density in the medium.

With incident optical field, the equation of motion can be presented by following equation.

$$m(\ddot{x} + \eta\dot{x} + \omega_0^2 x) = F(t) = \frac{1}{2} qE_0 e^{-i\omega t} \quad (2.3)$$

Where m is mass of electron, η is damping coefficient, ω_0 is natural resonance frequency of oscillator, E_0 is external electric field amplitude, ω is external electric field frequency. The solution of this equation is

$$x(t) = \frac{1}{2} \frac{e}{m} E_{amp} (\omega_0^2 - \omega^2 - i\eta\omega)^{-1} e^{-i\omega t} + c.c. \quad (2.4)$$

Therefore, the polarization is

$$P = Nqx = \frac{Ne^2}{2m} (\omega_0^2 - \omega^2 - i\eta\omega)^{-1} E_0 e^{-i\omega t} \quad (2.5)$$

Equation (2.5) shows that polarization is proportional to the electric field and in the same frequency. It is corresponding to linear optical phenomena. The theory of SHG can be presented by introducing anharmonic term ax^2 in to oscillator equation.

$$m(\ddot{x} + \eta\dot{x} + \omega_0^2 x + ax^2) = F(t) = \frac{1}{2} qE_0 e^{-i\omega t} \quad (2.6)$$

We assume ax^2 is small and solve the equation by perturbation theory. To simplify equation (2.6), we define

$$\begin{cases} L \equiv \frac{d^2}{dt^2} + \eta \frac{d}{dt} + \omega_0^2 \\ x \equiv x^{(1)} + x^{(2)} \\ F(t) = \frac{1}{2} qE_0 e^{-i\omega t} \end{cases} \quad (2.7)$$

Hence, equation (2.6) is revised as

$$Lx = \frac{F}{m} - ax^2 \quad (2.8)$$

Where $x^{(1)}$ is the solution of $Lx = \frac{F}{m}$. Accordingly $x^{(1)}$ is presented as

$$x^{(1)} = \frac{1}{2} X^{(1)}(\omega) e^{-i\omega t} + \frac{1}{2} X^{(1)}(-\omega) e^{i\omega t} \quad (2.9)$$

Where $X^{(1)}(\omega) = (\omega_0^2 - \omega^2 - i\eta\omega)^{-1}$. We keep the lowest order term of $x^{(2)}$

$$x^{(2)}(t) = \frac{1}{2} X^{(2)}(2\omega) e^{-i2\omega t} + \frac{1}{2} X^{(2)}(-2\omega) e^{i2\omega t} + X^{(2)}(0) \quad (2.10)$$

Where $X^{(2)}(\omega) = \frac{1}{2} L^{-1}(-2aX^{(1)}(\omega)^2)$.

From the first and second terms in equation (2.10), the frequency of oscillating electron is double that of incident electric field. In other words, SHG is revealed.

$$P(2\omega) = Nqx^{(2)} \quad (2.11)$$

2.1.1 Second order susceptibility

As mentioned before, with relatively low external field, the relationship between P and E is linear. The equation is given by

$$P = \varepsilon_0 \chi^{(1)} E \quad (2.12)$$

Compared with equation (2.5), $\chi^{(1)}$ could be declared as

$$\chi^{(1)} = \frac{1}{2\varepsilon_0} \frac{Nq^2}{m} \frac{e^{-i\omega t}}{(\omega_0^2 - \omega^2 - i\eta\omega)} \quad (2.13)$$

When applied field is strong enough, the relationship is not linear but can be expressed by a power series expansion.

$$P = \varepsilon_0 \chi^{(1)} E + \varepsilon_0 \chi^{(2)} E^2 + \varepsilon_0 \chi^{(3)} E^3 + \dots \quad (2.14)$$

These terms, except first one, imply nonlinear optical phenomena. With sinusoidal electric field $E(\mathbf{r}, t) = E_0 \cos(\omega t - \mathbf{k} \cdot \mathbf{r})$, equation (2.14) should be revised

$$P = \varepsilon_0 \chi^{(1)} E_0 \cos(\omega t - \mathbf{k} \cdot \mathbf{r}) + \varepsilon_0 \chi^{(2)} E_0^2 \cos^2(\omega t - \mathbf{k} \cdot \mathbf{r}) + \varepsilon_0 \chi^{(3)} E_0^3 \cos^3(\omega t - \mathbf{k} \cdot \mathbf{r}) + \dots \quad (2.15)$$

After using appropriate trigonometric operation, equation (2.15) becomes

$$P = \varepsilon_0 \chi^{(1)} E_0 \cos(\omega t - \mathbf{k} \cdot \mathbf{r}) + \frac{1}{2} \varepsilon_0 \chi^{(2)} E_0^2 [1 + \cos(2\omega t - 2\mathbf{k} \cdot \mathbf{r})] + \varepsilon_0 \chi^{(3)} E_0^3 \left[\frac{3}{4} \cos(\omega t - \mathbf{k} \cdot \mathbf{r}) + \frac{1}{4} \cos(3\omega t - 3\mathbf{k} \cdot \mathbf{r}) \right] + \dots \quad (2.16)$$

Obviously, there are new frequencies, which induced in nonlinear polarizations. Moreover, second term in equation (2.16) should be focused because it is linking to SHG.

$$P(2\omega) = \varepsilon_0 \chi^{(2)} E^2 \quad (2.17)$$

Similarly, by examining equation (2.11) and equation (2.17), second order susceptibility $\chi^{(2)}$ could be written as

$$\chi^{(2)}(2\omega, \omega, \omega) = -\frac{aNq^3}{\varepsilon_0 m^2} (\omega_0^2 - 4\omega^2 - i\eta 2\omega)^{-1} (\omega_0^2 - \omega^2 - i\eta\omega)^{-1} (\omega_0^2 - \omega^2 - i\eta\omega)^{-1} \quad (2.18)$$

In three-dimensional space, the direction of polarization and electric field should be considered. Hence, equation (2.17) can be rewritten as

$$P_i(2\omega) = \varepsilon_0 \chi_{ijk}^{(2)} E_j(\omega) E_k(\omega) \quad (2.19)$$

Thus $\chi_{ijk}^{(2)}$ is a third rank tensor and SHG efficiency is highly dependent on polarization of electric field.



2.1.2 Noncentrosymmetric organization

By coordinate transformation of $r \rightarrow -r$, second order polarization should be altered

$$P(2\omega) = \varepsilon_0 \chi^{(2)} E^2 \rightarrow -P(2\omega) = \varepsilon_0 \chi^{(2)} (-E)^2 \quad (2.20)$$

Clearly, equation (2.20) shows $P(2\omega) = -P(2\omega) = 0$ and $\chi^{(2)} = 0$. This result points to that SHG is forbidden in a centrosymmetric material. In the view of physics, it is because of destructive interference. Therefore, it is impossible to generate SHG in homogeneous material.

2.1.3 Phase matching condition

In order to enhance the conversion efficiency of SHG, momentum conservation is considered. In other word, the wavevectors of fundamental and second harmonic should be kept in special relationship:

$$\Delta k = k(2\omega) - 2k(\omega) \approx 0 \quad (2.21)$$

This situation is also called phase matching condition. Due to $k = 2\pi \frac{n\omega}{c}$ and

$v_{SHG} = 2v_{fundamental}$, phase matching condition can be revised as

$$n_{2\omega} \approx n_{\omega} \quad (2.22)$$

In this section, we consider the problem of phase matching in uniaxial medium, which exhibits two independent different refractive indices n_o and n_e . Former one called ordinary refractive index and we define $n_x = n_y = n_o$. Similarly, $n_z = n_e$, where n_e named extraordinary refractive index. If $n_e > n_o$, it is positive uniaxial crystal. Oppositely, it is called negative uniaxial crystal if

$n_e < n_o$. Accordingly, refractive index ellipsoid is drawn in Fig. 2.2 to determine the effective refractive index. The incident wavevector k is at angle θ with respect to Z axis and lies on Y-Z plane. Here, azimuthal angle is necessary due to rotational symmetry. If the polarization is parallel to the X-Y plane, the associated refractive index is n_o . Furthermore, if the polarization is parallel to the dashed line, which is perpendicular to X axis, the corresponding refractive index is $n_e(\theta)$, which is given by

$$n_e(\theta) = \left(\frac{\cos^2 \theta}{n_o} + \frac{\sin^2 \theta}{n_e} \right)^{-1/2} \quad (2.23)$$

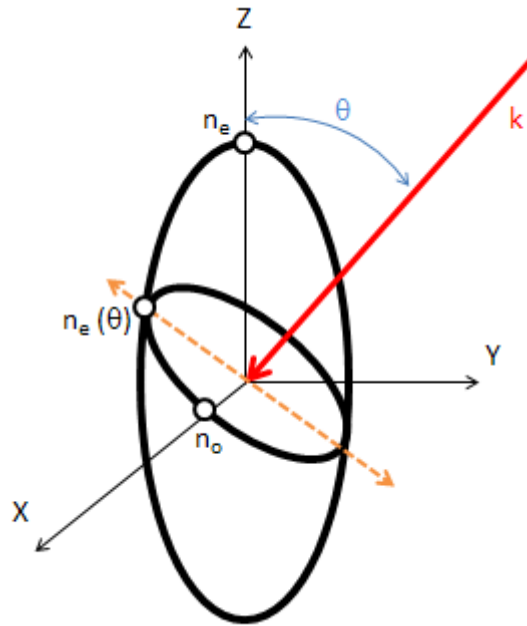


Fig. 2.2 refractive index ellipsoid in the uniaxial medium

Due to phase matching condition $n(2\omega) \approx n(\omega)$, SHG occurs in three types, denoted 0, I and II. In type 0 SHG, two photons with extraordinary polarization convert to a frequency-doubled photon with extraordinary polarization. In type I SHG, two photons with same polarization, which is ordinary or extraordinary polarization, will combine to form a photon with different polarization than two

original photons. In type II SHG, incident photons have ordinary and extraordinary polarization respectively.

As shown in Fig. 2.3, previous discuss about uniaxial medium provides a tunable refractive index and allows to generate SHG with different wavelength via changing the angle between polarization and orientation of material.

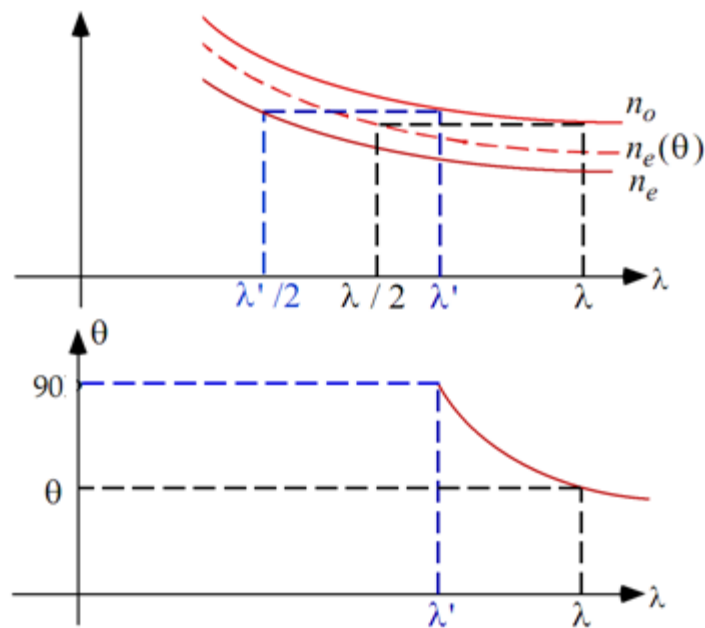


Fig. 2.3 The efficiency of SHG highly depends on the wavelength, polarization and orientation.

2.1.4 SHG in nematic liquid crystal

Nematic liquid crystal (NLC) is a well-known centrosymmetric material due to elastic theory [34]. From 2.1.2, it cannot generate SHG in matter with centrosymmetric due to destructive interference. Therefore, NLC should not present SHG, although it exhibits large refractive index anisotropy between its long and short axes. However, several different reports show strong SHG in well-aligned NLC cells, which is shown in Fig. 2.4 [35-38]. Several mechanisms

have been proposed to explain this contradictory phenomenon.

The first one is based on the electric quadrupole moment which allows all of three types SHG within centrosymmetric matter [39]. Considering the angle between the director of NLC and polarization of light, SHG signal should show four peaks. Nevertheless, it is usually very weak [36] because higher-order nonlinear susceptibility is very small. The other possibility is due to flexoelectric stress. When intense optical field is applied to NLC, light-induced curvature strains occur in NLC. Therefore, the centrosymmetry is broken by this deformation [36, 37, 39]. To sum up, NLC exhibits SHG, the efficiency of which is highly dependent on the angle between orientation of NLC and optical polarization [35, 36] For example, when the director of NLC is perpendicular to the propagation direction of light, the intensity of SHG could be presented as [39]

$$I \propto \cos^2 \theta \quad (2.24)$$

Where θ is the angle between director and the polarization of light.

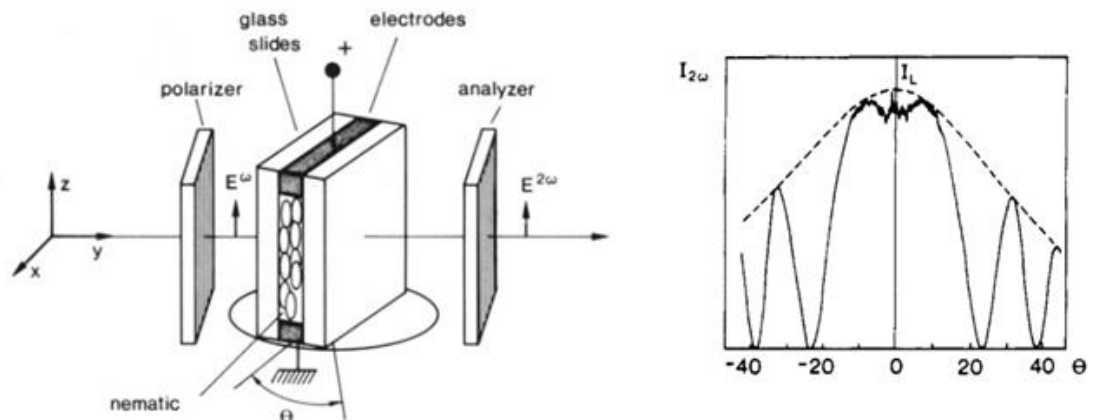
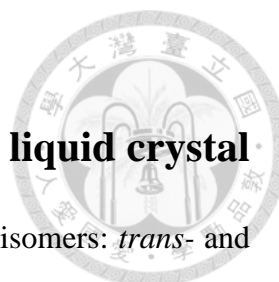


Fig. 2.4 the relationship between intensity of SHG and incident angle [37].



2.2 Light-induced transition in dye-doped liquid crystal

It is well known that azo-dyes can exist in two geometric isomers: *trans*- and *cis*-form dye. These two configurations can easily be interconverted by light and heat. As shown in Fig. 2.5, *trans* form dye is rod-like shape. On the other hand, the shape of *cis* one is bending. The isomerization processes, which is reversible, is induced by the electronic excitation of an electron from either the highest occupied nonbonded orbital or the highest occupied π orbital to the lowest unoccupied π orbital. Because the *trans* dye lies lower in energy level, *cis* dye relaxes to *trans* dye spontaneously. Typically, both photo-chemical conversions occur on a picosecond time scale. However, the thermal relaxation from *cis* form to *trans* form is ranging from millisecond to second [22].

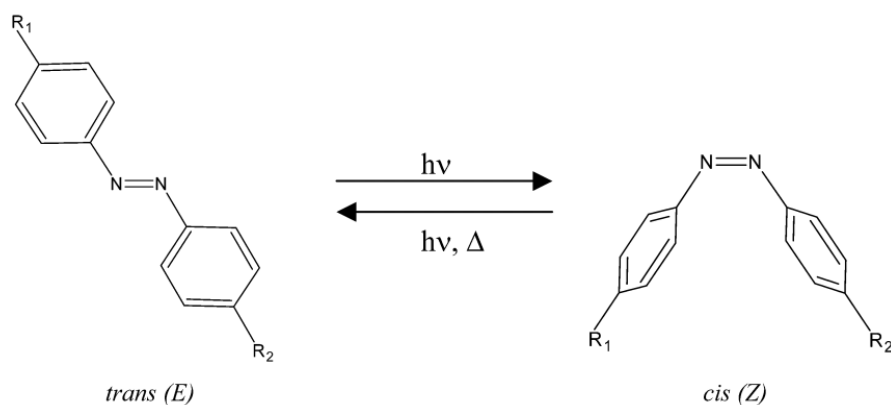


Fig. 2.5 Reversible optical switch between *trans*- and *cis*-azo-dye [22]

In the past few decades, some researcher found that the properties of liquid crystal are changed by mixing with a small amount of azo-dye, which is called dye-doped liquid crystal (DDLC). To demonstrate controllable SHG in DDLC, second order susceptibility should be altered. Here, we raise two possible mechanisms of optical controllable SHG and azo-dye may play important roles

among them. The first one is optical Fredericks transition, and the other one is nematic-isotropic phase transition.



2.2.1 Optical Fredericks transition

As we mentioned that LC exhibits large refractive index anisotropy, the molecule can be reoriented by external electric field. This phenomenon, called Fredericks transition, is due to the nonhomogeneous electron distribution. Its applications are found in many fields such as display technologies. Similarly, the orientation of LC can also be controlled by optical field and is named OFT. By OFT and relationship between orientation and polarization, it is possible to demonstrate optical controllable SHG.

The main principle of OFT is optical-induced torque. The volume torque Γ is

$$\Gamma = \varepsilon_0 \varepsilon_a (\mathbf{n} \cdot \mathbf{E})(\mathbf{n} \times \mathbf{E}) \quad (2.25)$$

Where \mathbf{n} is the nematic director, ε_0 is electric permittivity of free space, \mathbf{E} is the electric field, $\varepsilon_a = n_e^2 - n_o^2$. n_e and n_o are the extraordinary and ordinary refractive indices respectively.

In the 1990s, Janossy claimed OFT torque can be enhanced by doping LC with a small amount of azo-dye [27]. In other words, OFT threshold is lower than pure sample. For instance, it is reported that nematic LC mix with 1% of 1% of 1,8-dihydroxy, 4,5diamino, 2,7 diisopentyl-anthraquinone reduces the OFT threshold by two orders of magnitude [25]. This dye-induced torque has same form as the time-averaged optical torque:

$$\Gamma_{dye} = \eta \langle \Gamma \rangle \quad (2.26)$$

And we can arrange equation(2.26):

$$\Gamma_{dye} = \eta \epsilon_0 \epsilon_a \langle (\mathbf{n} \cdot \mathbf{E})(\mathbf{n} \times \mathbf{E}) \rangle \quad (2.27)$$

Where η is a dimensionless factor and due to the interaction between excited dye and LC. Therefore, η is related to the concentration of *trans*- and *cis*-dye.

This dye-enhanced torque is not due to the nonhomogeneous electron distribution but the structural change of azo-dye and the interaction between dyes and LC molecules. When this rod-like dyes are dissolved in LC, the molecules will orient aligned with LC. However, if DDLC sample is illuminated, it changes the structure of azo-dye from rod-like to bend-shape. this structural change also reoriented the LC molecules. Since the efficiency of SHG is highly dependent on the angular relationship between polarization and orientation of molecules, controllable SHG can be realized by this dye-induced reorientation. Besides, after *cis* dye relaxes to *trans* dye, the *trans* form will tend to rotate LC to original direction. So the SHG is alterable by control the concentrate of *trans*- and *cis*-dye.

2.2.2 Nematic-isotropic phase transition

As we known the isotropic phase is a homogenous state. Therefore, due to the property of centrosymmetry, SHG is not allowed in isotropic phase. So it is possible to demonstrate optical controllable SHG by phase transition between nematic and isotropic.

Nevertheless, it needs high optical intensity to induce phase transition in pure LC film. It is reported the phase transition temperature is reduced by mixing a small amount of azo dye into LC [28]. Because *trans* dye is rod-like, it is more stable in LC than its isomer, which is bent-shape. As a result, the

nematic-isotropic phase transition temperature of the mixture with the *cis* form (T_{cc}) is much lower than that with the *trans* form (T_{ct}), as shown in Fig. 2.6. So it can reduce the threshold of light-induced nematic-isotropic phase transition. If DDLC sample is irradiated to cause *trans*–*cis* photoisomerization of the azo-dyes, due to lower transition temperature, the nematic-isotropic phase transition will occur. On the other hand, the isomerization is reversible, so the LC sample reverts to nematic phase spontaneously. It means SHG is controllable by the dye-induced phase transition.

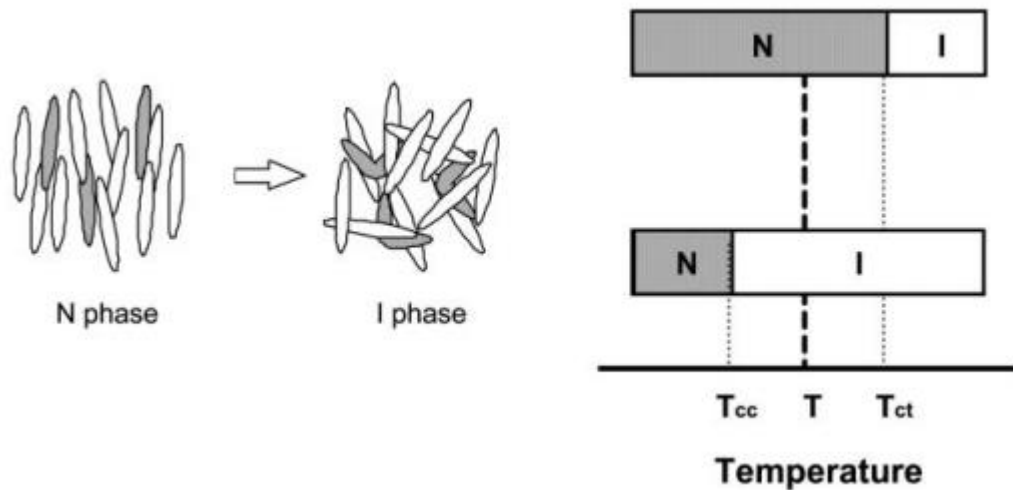
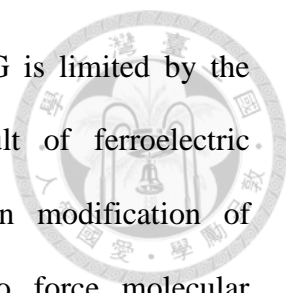


Fig. 2.6 Phase transition of DDLC. N, nematic; I, isotropic[28]. T_{ct} and T_{cc} are the nematic-isotropic phase transition temperature of the mixture with the *trans*- and *cis* form

2.2.3 Potential of DDLC-based optically controllable SHG

Previously, optically controllable SHG has been demonstrated in poled polymers containing photochromic dyes [15, 16], organic photochromic crystals [17, 18] and two-photon isomerization of azobenzene moieties in cross-linked ferroelectric liquid-crystalline polymers[19]. However, there are several



drawbacks. The response time of optically controllable SHG is limited by the reaction rate of photochromic reaction. Except the result of ferroelectric liquid-crystalline polymers, the mechanisms are based on modification of molecular hyperpolarizability. However, it is not easy to force molecular hyperpolarizability to zero. Therefore, contrasts are less than 50%. Besides, controllable SHG in poled polymers faces the problem of irreversible changes in the initial chromophore alignment after several switches. It limits the number of on-off cycles of SHG.

In contrast, DDLC-based optically controllable SHG has high potential to overcome these disadvantages, including long response time, low on-off contrast and irreversible switch. Following is a brief explanation.

First, the response time of both LC and azo dye is in second scale or less. Thus, DDLC might be a demonstration of high-speed SHG switch. Second, both of possible mechanisms mentioned in 2.2.1 and 2.2.2 is based on molecular dynamics instead of hyperpolarizability. Therefore, the contrast could be higher than previous results. Finally, SHG should not decrease after several switch cycles because there is no chemical reaction in liquid crystal.

2.3 Microscopic application

2.3.1 Confocal microscopy

Optical microscopy provides a non-invasive observation method and is useful in many different fields, biology especially. However, in wide-field microscopes, when intense laser is tightly focused on the sample, the signal from out-of-focus plane is collected and blurs the image. As a result, image with low optical

resolution and high background is detected. Combined with scanning system and motorized Z-stage, it enables reconstruction of three-dimensional structures.

Therefore, to avoid this drawback, confocal microscopy was invented by Marvin Minsky in 1957. In Fig. 2.7, point illumination and confocal pinhole, which is placed in an optical conjugate plane in front of the detector, are required in confocal microscope. Under this setup, out-of-focus signal is blocked and eliminated by confocal pinhole. As a result, the signal-to-background ratio, particularly in axial direction, and signal-to-noise ratio are improved. It enables the reconstruction of three-dimensional image. However, compared with traditional wide-field microscope, it suffers from lower signal acquisition due to confocal pinhole. Moreover, this point-scan method is much slower because it is illuminated at a time.

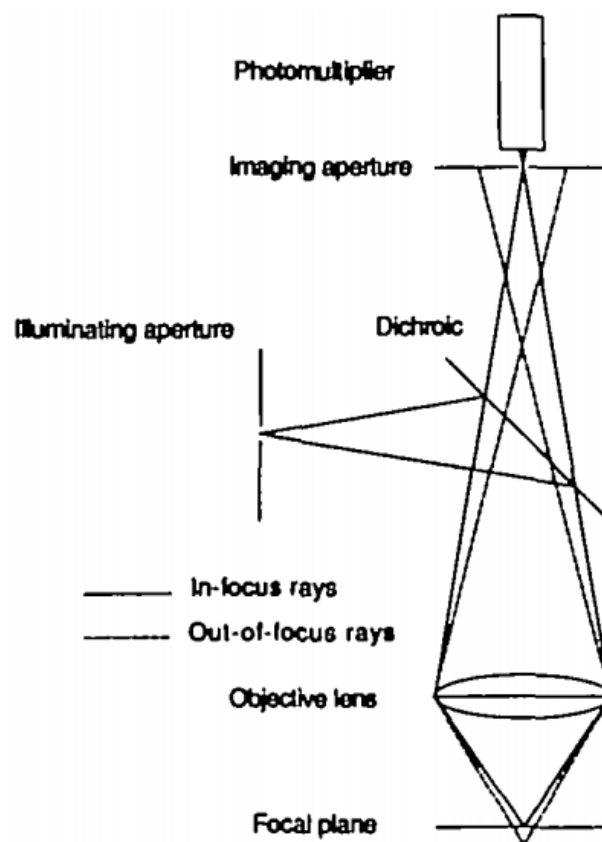


Fig. 2.7 Scheme of confocal microscope [40]

To construct an image from confocal microscope, a moving focal spot should scan across the sample. There are several ways of scan including scanned beam, scanned stage and scanned pinhole[40]. First scanned beam method use multiple mirrors or acousto-optic. This method has advantage in scan speed but the image is distorted in the edge. Scanned stage is a method with moving specimen and fixed incident light. Due to constant axial illumination, optical aberration is reduced. However, the scan rate is very slow. Last method, scanned pinhole, equipped Nipkow spinning disk, a rotational set with multiple sets of pinholes, in the conjugate plane. With fast acquisition rate, it has disadvantage in low incident efficiency and distortion. In this thesis, both scanned beam, scanned stage are used.

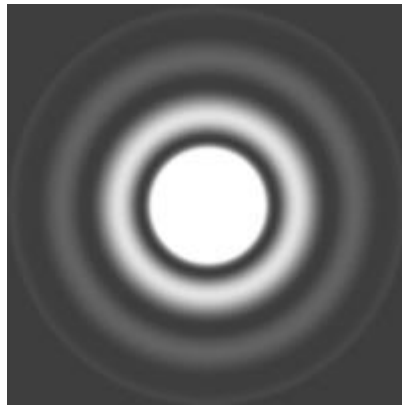
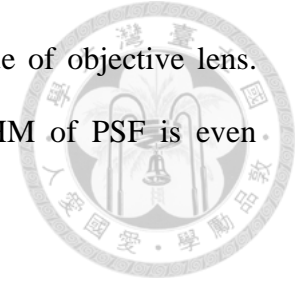


Fig. 2.8 Airy disk

The energy distribution at focal plane produced by a point light source is called point spread function (PSF). The intensity profile is represented by an Airy disk (see Fig. 2.8) and considered as the resolution of microscope. Thanks to Ernst Abbe, the size of PSF is limit by diffraction and the full width at half maximum (FWHM) of PSF is

$$d \cong \frac{0.61\lambda}{NA} \quad (2.28)$$

Where λ is wavelength and NA is numerical aperture value of objective lens. Furthermore, in the case of confocal microscope, the FWHM of PSF is even narrower because of confocal pinhole [41].



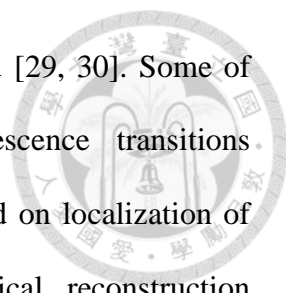
$$d_c \cong \frac{0.44\lambda}{NA} \quad (2.29)$$

2.3.2 Second harmonic generation (SHG) microscopy

In 1974, SHG microscopy is first reported by Hellwarth and Christensen [42]. Because SHG is proportional to square of incident intensity, it only occurs near the focal spot. In other words, due to avoiding the signal from out-of-focus plane, SHG microscope permits intrinsic optical section without confocal pinhole. It means the collection efficiency is better than traditional confocal microscope. The axial resolution of SHG microscopy is in sub-micrometer scale and comparable to confocal microscopy. In addition, near-infrared laser is usually used in SHG microscopy. Due to lower scattering for longer wavelength, SHG microscopy also provides long penetration depth, which is up to several hundred micrometers. Since many biological structures exhibit strong SHG signals and is thick, SHG microscopy, which allows non-invasive and blur-free three-dimensional image, is used to observation of living species [43, 44].

2.3.3 Overview of superresolution microscopy

Although traditional optical microscopy provides a real-time, non-invasive and 3-dimensional observation and is widely used to examine biological specimens, it is limited by relatively low spatial resolution, mentioned in equation (2.29), due to diffraction of light. Thus, to overcome diffraction barrier, a number



of superresolution microscopy techniques have been invented [29, 30]. Some of them, categorized as reversible saturable optical fluorescence transitions (RESOLFT) [30], based on sharpening the PSF. Others based on localization of individual fluorescent molecules including stochastic optical reconstruction microscopy (STORM) [45] and photoactivated localization microscopy (PALM) [46].

In RESOLFT, PSF sharpened by another donut-shape light, which turns off the signal in peripheral region of focal spot. In other words, the basic idea of RESOLFT is optically switchable and reversible mechanism. For example, stimulated emission depletion (STED) microscopy, one of the most successful RESOLFT, uses high-intensity light to switch off the fluorescence in peripheral part of focal spot and narrows the effective PSF via stimulated emission.

On the other hand, localization microscopies improve resolution by stochastically switching of fluorescence via photoactivation, photoconversion or photoswitching. Then, reconstructing the high-resolution image by localization calculation.

To realize superresolution based on optically controllable SHG, localization microscope is not an ideal method because its core mechanism, stochastically switching, is not happened in our demonstration. In contrast, it has very high potential to fulfill RESOLFT-like superresolution microscope by optically controllable SHG. Therefore, the details of RESOLFT microscope will be discussed in 2.3.4.

2.3.4 Reversible saturable optical fluorescence transitions (RESOLFT) microscope



Follow to last section, RESOLFT-like superresolution technique may be an application of our studies, optically controllable SHG. Thus, the principle of RESOLFT microscope will be shown in this section.

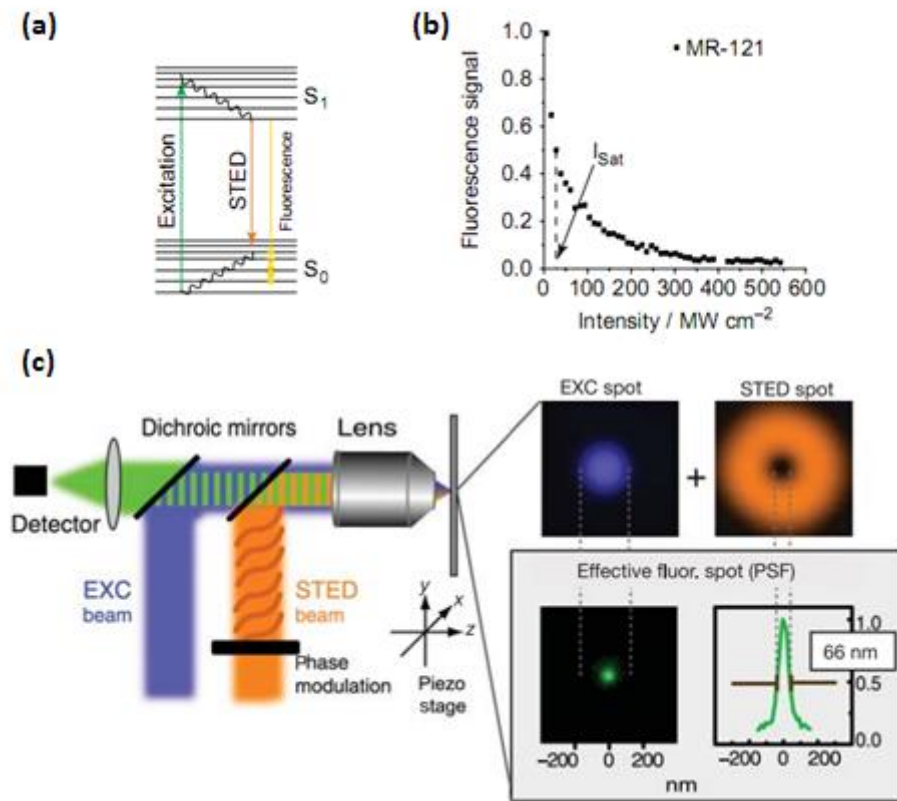


Fig. 2.9 The concept of STED. (a) Energy diagram, (b) depletion curve and (c) Setup of STED [47, 48]

The principle of RESOLFT microscope is combining two lights, excitation beam and depletion beam, the former one is used to excite electrons of fluorophores. Generally, electrons relax from excited state to ground state spontaneously and generate fluorescence. However, with intense depletion beam, the electrons in excited state are enforced to other state. Therefore, the fluorescence signal is turned off. The depletion beam, which passes through phase

modulation, is doughnut-shape and depleted the fluorescence in peripheral region and narrows the effective PSF of excitation beam, namely resolution is enhanced. In Fig. 2.9, STED microscope is taken as example. In STED microscope, depletion light is also called STED light, which turns the fluorescence off via stimulated emission.

To derive the enhanced resolution, first of all, we need to define fluorescence probability $\eta(x)$, or depletion factor from Fig. 2.9(b).

$$\eta(x) = e^{-\sigma\tau I_{dep}(x)} \quad (2.30)$$

Where x is the coordinate in the focal plane. σ and τ denote the cross section for stimulated emission and lifetime of fluorescence respectively. $I_{dep}(x)$ means the intensity of STED beam in position x . To simplify the calculation, as shown in Fig. 2.10, it is suggested to be approximated by a parabola with its minimum at the focal point [49, 50]:

$$I_{dep}(x) = 4I_{Dep}a^2x^2 \quad (2.31)$$

Where I_{Dep} means the total intensity of depletion light, a is the steepness factor.

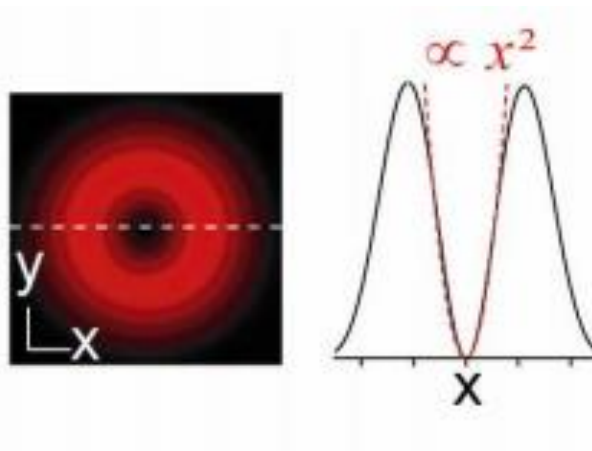


Fig. 2.10 parabolic approximation of depletion beam [49]

Then, we assume the $h_{exc}(x)$ is the normalized excitation probability in the focal plane resulting from the excitation beam without depletion beam. It means the probability of detecting photon from position x . Generally, $h_{exc}(x)$ follows Gaussian distribution and define the conventional resolution, which is discussed in previous section. Thus $h_{exc}(x)$ is defined as

$$h_{exc}(x) = 2 \frac{4x^2}{d_c^2} = e^{-4 \ln(2) \left(\frac{x}{d_c}\right)^2} \quad (2.32)$$

Here, d_c means the FWHM of focal spot in a confocal microscope, namely the resolution.

Thus, the new excitation probability is

$$\begin{aligned} h(x) &= h_{exc}(x) \cdot \eta(x) \\ &= e^{-4 \ln(2) x^2 \left(d_c^{-2} + a^2 \frac{I_{Dep}}{I_{sat}} \right)} \end{aligned} \quad (2.33)$$

Where I_{sat} is saturation intensity, which is defined as the intensity of depletion light required when half of the fluorescence is suppressed. It is proportional to $1/\sigma\tau$. Thus the FWHM of enhanced PSF is

$$d_{STED} = d_c / \sqrt{1 + d_c^2 \cdot a^2 \cdot \zeta} \quad (2.34)$$

Where $\zeta \equiv \frac{I_{Dep}}{I_{sat}}$. It is obvious that ζ and a dominate the resolution of STED microscopy. Former one is shown in Fig. 2.11.

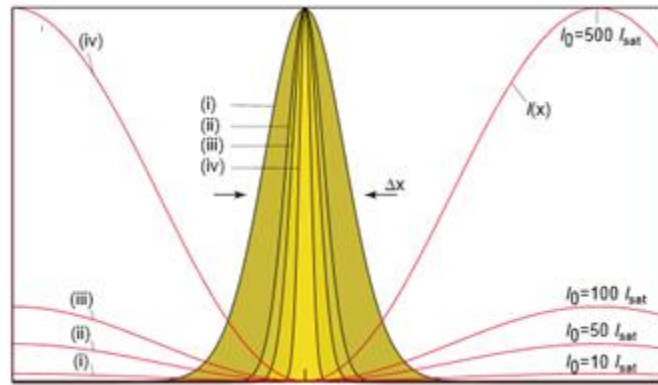


Fig. 2.11 the relationship between effective PSF and $\zeta (\equiv \frac{I_{Dep}}{I_{sat}})$ [47]

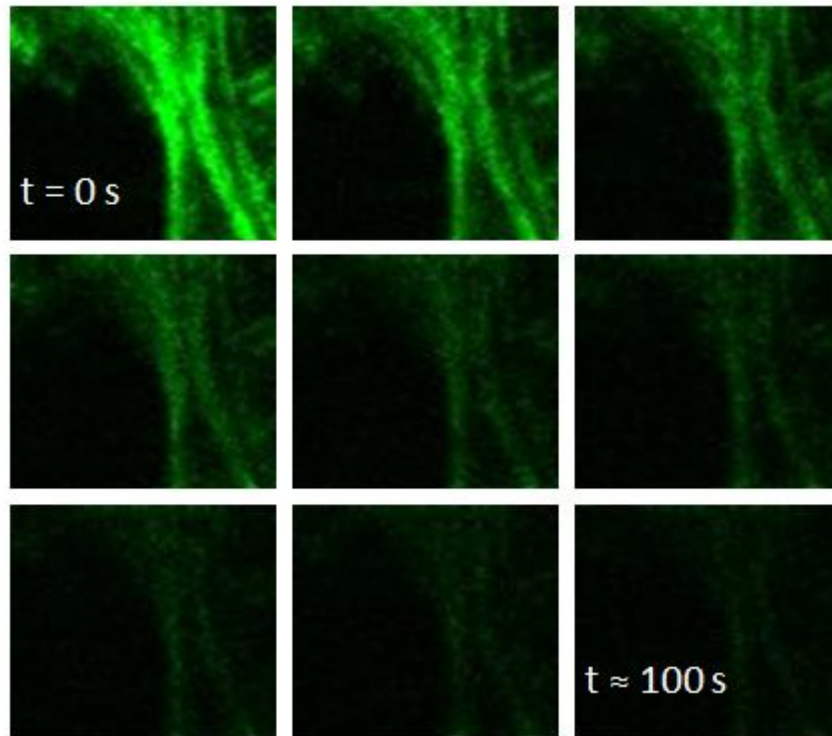


Fig. 2.12 Photobleaching demonstration on actin of melanin cell stained by

$$\text{Alexa-488 } (I \cong 10^7 \text{ W/cm}^2)$$

However, with high-intensity illumination, the fluorescence signal may decrease dramatically as time passes. This phenomenon, called photobleaching, is due to photochemical destruction of a fluorophores and shown in Fig. 2.12.

Therefore, non-bleaching technique becomes a new aim of superresolution

microscopy [32, 33].

Our studies is optical controllable SHG, namely SHG signal is switchable and reversible by light. It reveals that this work maybe can apply to RESOLFT-like superresolution microscope. Because the mechanism is not fluorescence, it does not suffer from photobleaching. So it may be a solution of non-bleaching microscopy.



Chapter 3 Sample and method



3.1 DDLC Sample (special thanks to Prof Chih-Yu Chao and his student, Chao-Ran Wang, for preparing sample)

Our samples are dye-doped liquid crystal (DDLC) cells, which is NLC mixed with a little amount of azo dye. Azo dye and NLC used for fabricating LC cell are disperse red 1 (DR1) (Sigma-Aldrich, US) and MDA-98-1602 (Merck, US). The content ratio between NLC and azo dye is 99:1. After shaking the mixture of NLC and DR1, it is injected into the empty cell, covered by glasses coated with pre-aligned polymers. In order to generate stronger SHG, anti-parallel arrangement is chosen [51]. Besides, the orientation of DDLC is restricted to be identical by the arrangement. There are several different cell gaps in our sample including 1.5, 8 and 20 μm . On the other hand, DR1 exhibits two absorption peaks. One locates at UV region. The other one is around 500 nm [52].

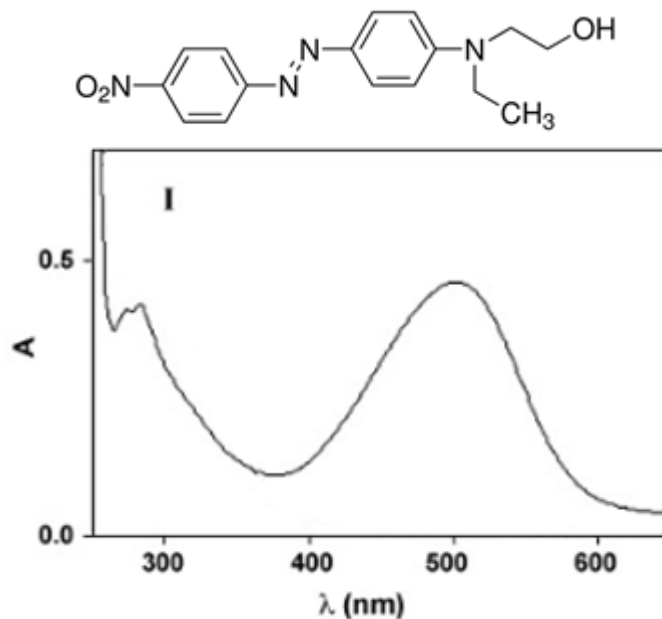
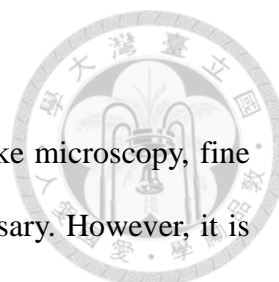


Fig. 3.1 structural formula and spectra [52] of DR1



The preparation procedures of cell are lists as followed:

- Clean the glasses
 1. Glasses are sonicated in detergent for 30 minutes.
 2. Scrub the glasses, and sonicate them in detergent for 30minutes again.
 3. Put glasses in deionized water and sonicate them for 10 minutes twice.
 4. In order to remove water, glasses is put in oven and heated to 100 °C for 10 minutes.
- Prepare glass with alignment layer
 1. By spin coating, pre-aligned polymer solution covers over the glasses.
 2. Solidify the polymer by heating to 80 °C and then 230 °C for 10 minutes and 1 hour respectively.
 3. To prepare alignment, rub the polymer layer.
- Assemble cell
 1. Put spacers on a glass. Then, cover it by another glass
 2. Apply ultraviolet resins to one edge of cell.
 3. To solidify ultraviolet resins, the cell is illuminated by ultraviolet for 1 minute.
 4. Apply ultraviolet resins to opposite edge of cell.
 5. To solidify ultraviolet resins, the cell is illuminated by ultraviolet for 1 minute.
- Inject LC into cell
 1. Mix LC with a little amount of azo dye. The content ratio between NLC and azo dye is 99:1
 2. Heat and sonicate DDLC until azo dye dissolve.
 3. Inject DDLC into cell



3.1.1 Fine structure

To analysis the resolution improvement of RESOLFT-like microscopy, fine structure, which size should be smaller than 100 nm, is necessary. However, it is hard to find such small structure in normal LC cell. Therefore, we did some special treatments for this aim.

Nano-gold-doped sample

As shown in Fig. 3.2, a glass coated with pre-aligned polymer is replace by the one covered by 80-nm gold nanoparticles. There are reports of SHG from gold nanoparticles are local surface contribution [53, 54]. Compared to SHG from NLC, SHG from nanoparticles is very weak. It means nanoparticles look dark in SHG image. Thus, resolution could be confirmed by detect the image around the gold nanoparticle.

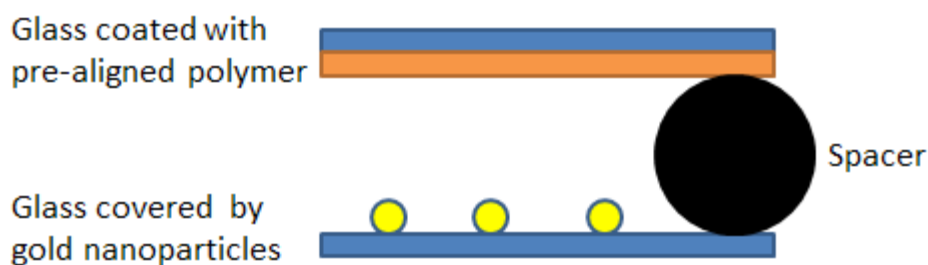


Fig. 3.2 Sectional drawing of nano-gold-doped sample

Here are the preparation procedures of nano-gold-doped cell

- Clean the glasses
Refer to “Clean glasses” in 3.1
- Prepare glass with alignment layer
Refer to “Prepare glass with alignment layer” in 3.1
- Prepare glass with gold nanoparticle



1. Gold nanoparticle colloid solution is sonicated for 15 minutes for preventing aggregation of nanoparticles.
 2. Gold nanoparticle colloid is dropped on glass and then kept drying naturally in clean room for 20 minutes.
 3. To prevent multi-layer accumulated gold nanoparticle, extra colloid is removed by deionized water washing.
 4. Get rid of remaining distilled water by nitrogen gas
- Assemble cell
 1. Put spacers on the glass with nanoparticle. Then, cover it by glass with alignment layer
 2. Apply ultraviolet resins to one edge of cell.
 3. To solidify ultraviolet resins, the cell is illuminated by ultraviolet for 1 minute.
 4. Apply ultraviolet resins to opposite edge of cell.
 5. To solidify ultraviolet resins, the cell is illuminated by ultraviolet for 1 minute.
 - Inject LC into cell

Refer to “Inject LC into cell” in 3.1

Artificial structure made by photoresist

In this sample, one glass is coated with photoresist. In Fig. 3.3, there are two rectangular holes ($5 \times 20 \text{ nm}^2$) on photoresist layer by dissolving after UV-illumination. Therefore, from the edge of photoresist, the resolution could be determined.

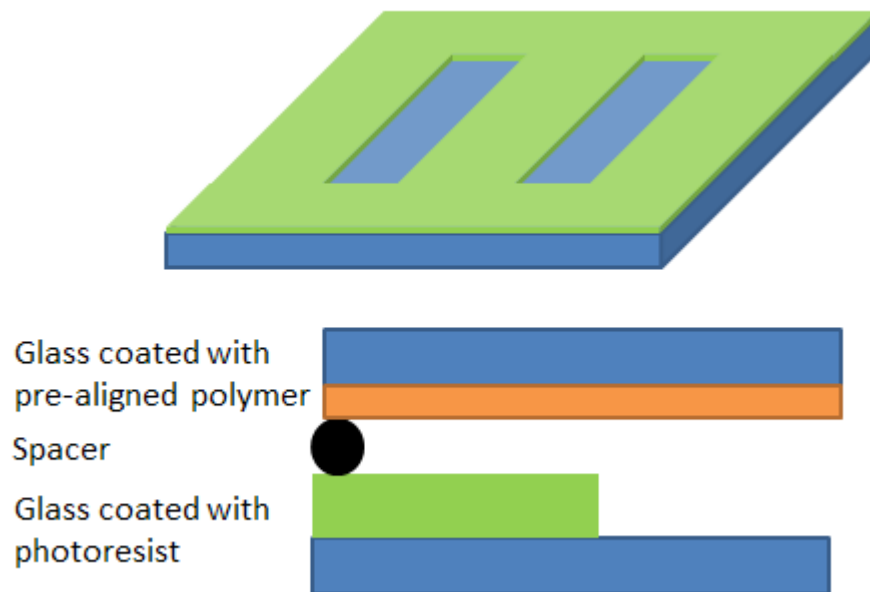
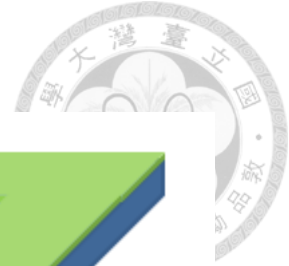
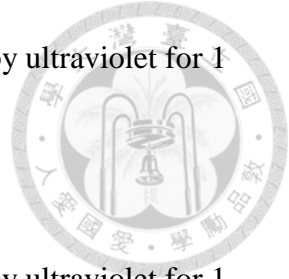


Fig. 3.3 The glass coated with photoresist and the cross-sectional drawing of cell

Following are the preparation procedures of artificial-structure sample

- Clean the glasses
Refer to “Clean glasses” in 3.1
- Prepare glass with alignment layer
Refer to “Prepare glass with alignment layer” in 3.1
- Prepare glass with artificial-structure
 1. By spin coating, photoresist covers over the glasses
 2. Glasses are exposed to UV and sonicated in developer. Then, photoresist at the exposed region dissolve. As a result, there are two rectangular holes.
- Assemble cell
 1. Put spacers on the glass with nanoparticle. Then, cover it by glass with alignment layer
 2. Apply ultraviolet resins to one edge of cell.



3. To solidify ultraviolet resins, the cell is illuminated by ultraviolet for 1 minute.
 4. Apply ultraviolet resins to opposite edge of cell.
 5. To solidify ultraviolet resins, the cell is illuminated by ultraviolet for 1 minute.
- Inject LC into cell
Refer to “Inject LC into cell” in 3.1

3.2 Polarized light microscope

To verify the mechanism of optical Fredericks transition (OFT) or phase transition, polarized light microscope is an ideal method. As we show in Fig. 3.4, there are two laser sources. One is a continuous wave diode laser, emitting at $\lambda = 473$ nm, and used as control light. The other one (iBeam-smart-785-S, Toptica, Germany) is probe light. We put two polarizing beam splitters (PBS) (PBSH-450-1300-050, CVI, Germany) under the objective (UPlanSApo 20x/0.75, Olympus, Japan) and above the condenser (IX2-DICD, Olympus, Japan) respectively. In this experiment, rubbing direction and the orientation of sample are parallel or perpendicular to the PBS under objective. Therefore, without control light, the polarization of probe light should not be rotated by sample.

In OFT case, the orientation of NLC is reoriented by control light. Hence, the polarization of probe light is changed, too. So, the intensity of probe light decreases. On the other hand, if the mechanism is phase transition, polarization of probe light would not be altered by isotropic state. In other words, the intensity of probe light is not changed by control light. To sum up, we can determine the

mechanism by measuring the intensity after second PBS and filters (CG-OG-570, CG-RG-630, CVI, Germany).

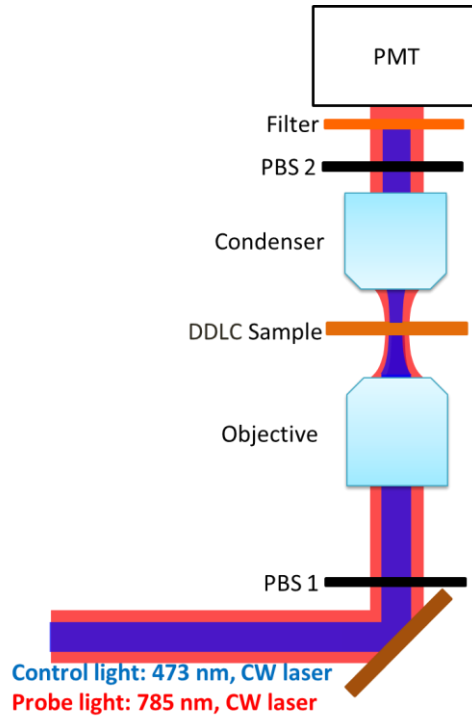


Fig. 3.4 Polarized light microscope setup

3.3 RESOLFT-like SHG microscopy

3.3.1 Setup

Fig. 3.5 shows the setup. There are two different lasers. Similar to the previous section, 473-nm continuous wave (CW) diode laser is the control light. It is used to alter the orientation or phase of NLC and control the intensity of SHG. In order to change the incident intensity, there is a ND filter in the path of control light. The other one is a near-infrared (IR) ultrafast laser (Uranus 005, Polar Onyx, CA) to generate SHG in DDLC. Here we use a telescope system to make sure both lasers focus on same surface of sample. Both of them pass through half-wave

plates (AHWP05M-600, THORLABS, US; 10RP02-32, Newport, US) and a polarizing beam splitter (PBSH-450-1300-050, CVI, Germany) to make sure all of them are in same polarization. Moreover, we put an iris to alter the incident beam size. To focus the beams and collect the transmitted light or SHG, an objective (UPlanSApo 20x/0.75, Olympus, Japan) and a condenser (IX2-DICD, Olympus, Japan) are used respectively. After passing through a filter set (BG-39, CVI, Germany, TBP01-550/15, FF01-520/15-25, FF01-525/30, Semrock, US), the signal is detected by a photomultiplier tube (PMT) (PMC-100, Becker & Hickl GmbH, Germany) of time-correlated single photon counting (TCSPC), which will be described in the next section.

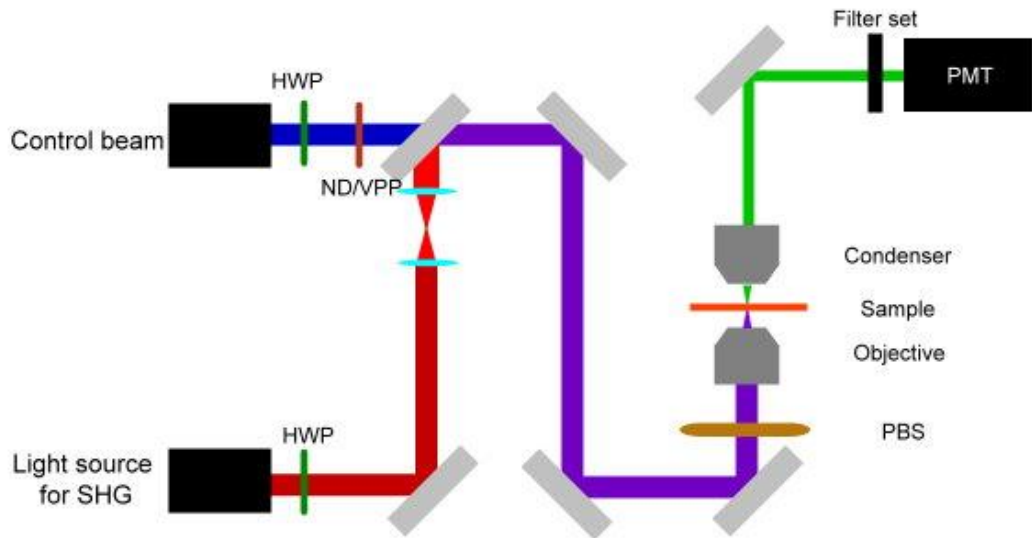


Fig. 3.5 Setup

To realize superresolution based on controllable SHG, control light should be transformed into a doughnut-shape beam. Thus, ND filter is replaced by a vortex phase plate (VPP) (VPP1-b, RPC, US). By switching off SHG signal in periphery region, resolution is improved. In addition, due to the limit of response

time of transition, the scanning rate should be slow enough. Therefore, instead of mirror-based scanner, scanning stage (P-545.3R2, PI, Germany) is used to get superresolution image. To synchronize scanning stage with TCSPC system, as shown in Fig. 3.6, a data acquisition (DAQ) card (USB-6211, National Instruments, US) is used to provide pixel, line and frame clock.

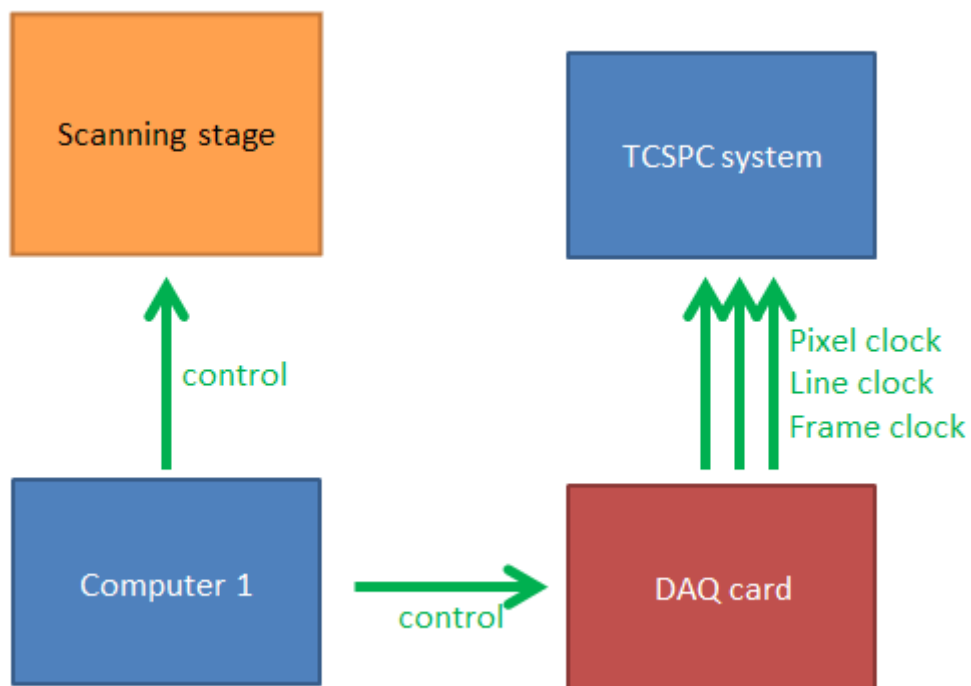


Fig. 3.6 Scheme of synchronizing scanning stage and TCSPC system

3.3.2 Time-correlated single photon counting (TCSPC)

Unfortunately, from Fig. 3.1, azo dye exhibits fluorescence around 500 to 600 nm while the wavelength of SHG is 520 nm. Therefore, time-correlated single photon counting (TCSPC) system is used to temporally distinguish SHG from fluorescence.

The basic idea of TCSPC is based on the detection of single photons of a periodic light signal, the measurement of the detection times, and the

reconstruction of the waveform from the individual time measurements. As shown in Fig. 3.7, fluorescence is periodically excited by a pulse laser. As an example, the repetition rate of laser is 80 MHz (Fig. 3.7-a). The expected fluorescence is shown in Fig. 3.7-b. However, due to the limit of detection rate and weak signal, the detector signal (Fig. 3.7-c) does not correspond to the expected fluorescence.

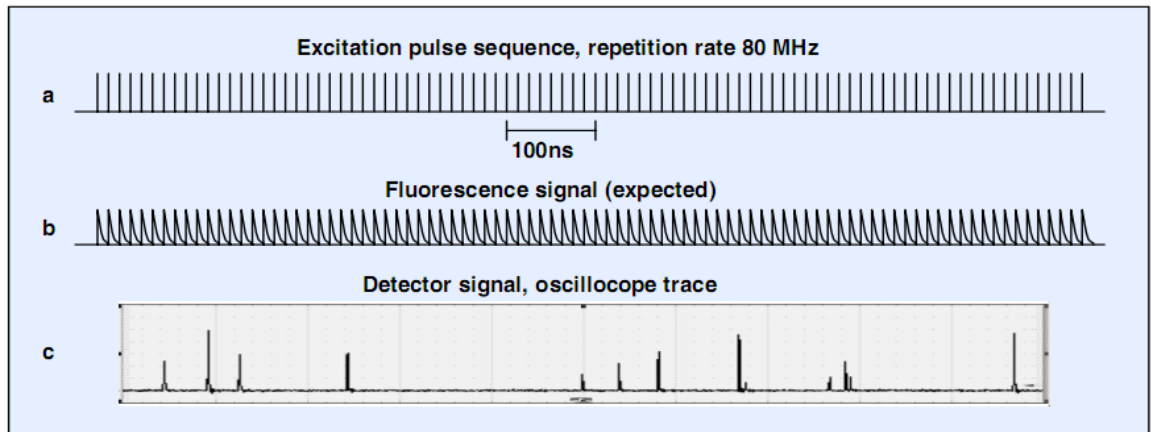


Fig. 3.7 Detector signal for fluorescence detection at a pulse repetition rate of 80 MHz

To reconstruct the waveform of fluorescence, a reference pulse from light source is necessary (Fig. 3.8). Hence, the arrival time of every photon is determined by interval between detector signal and reference signal. After many signal periods, a large number of photons are detected. Then, as shown in Fig. 3.9, the distribution of photons is build up. It could be considered as the waveform of fluorescence in a single period due to stable repetition rate of pulse laser and single photon counting.

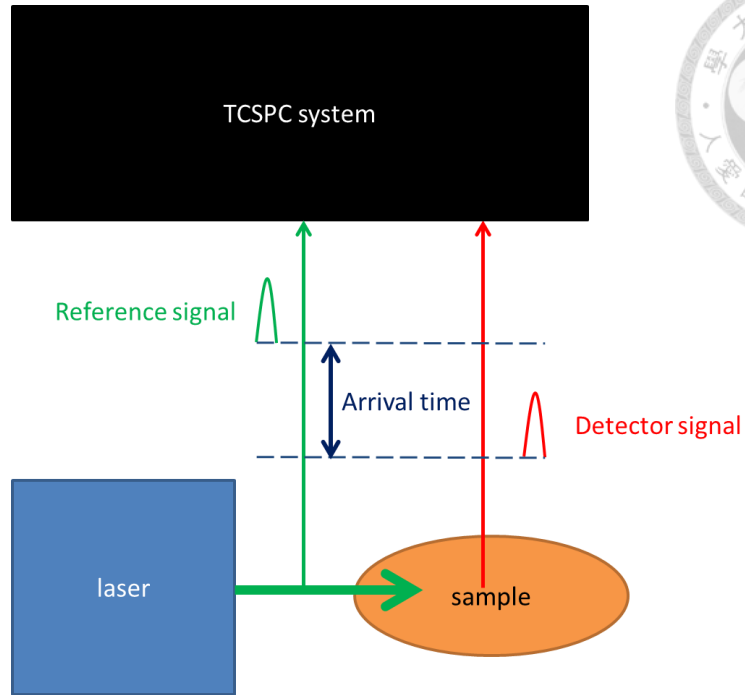


Fig. 3.8 Relationship between reference and detector signal

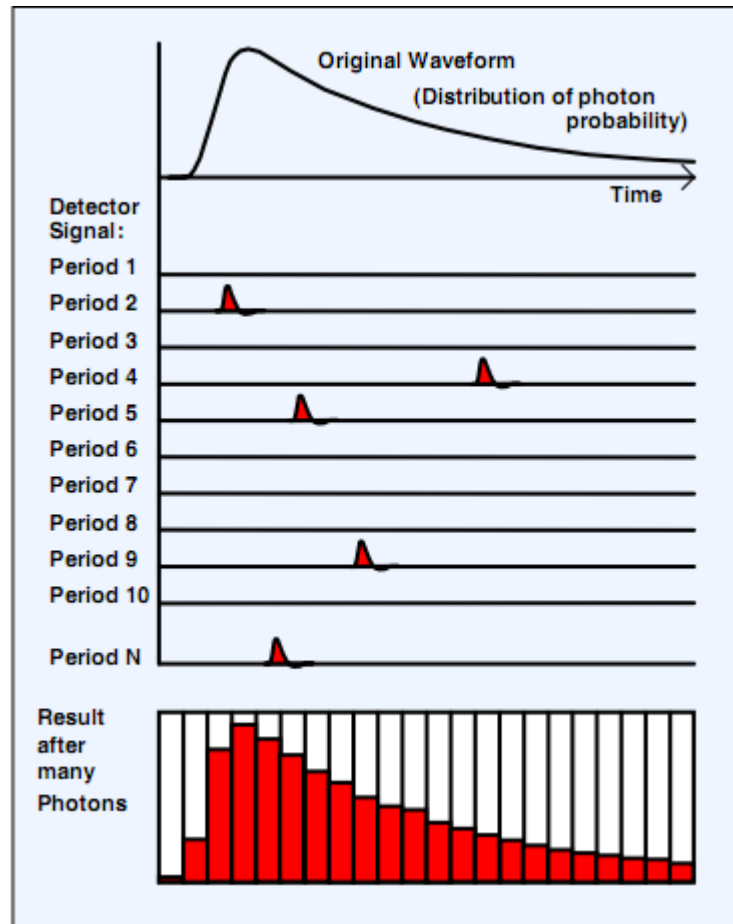


Fig. 3.9 Principle of reconstructing waveform

Back to our case, as shown in Fig. 3.10, SHG, whose lifetime is extremely short, is a pulsed signal following the excitation laser. On the other hand, the fluorescence, which is excited by CW laser, is not related to time. Thus, we can separate SHG signal from fluorescence by TCSPC system.

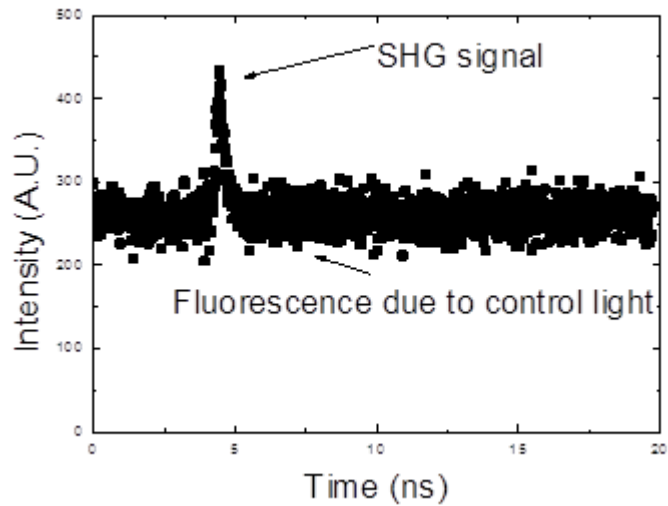
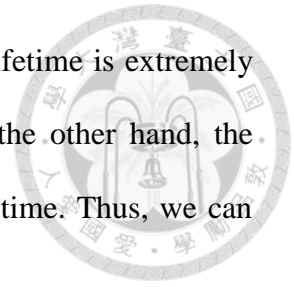


Fig. 3.10 Distinguish SHG signal from fluorescence

Chapter 4 Results and discussion



4.1 SHG in DDLC

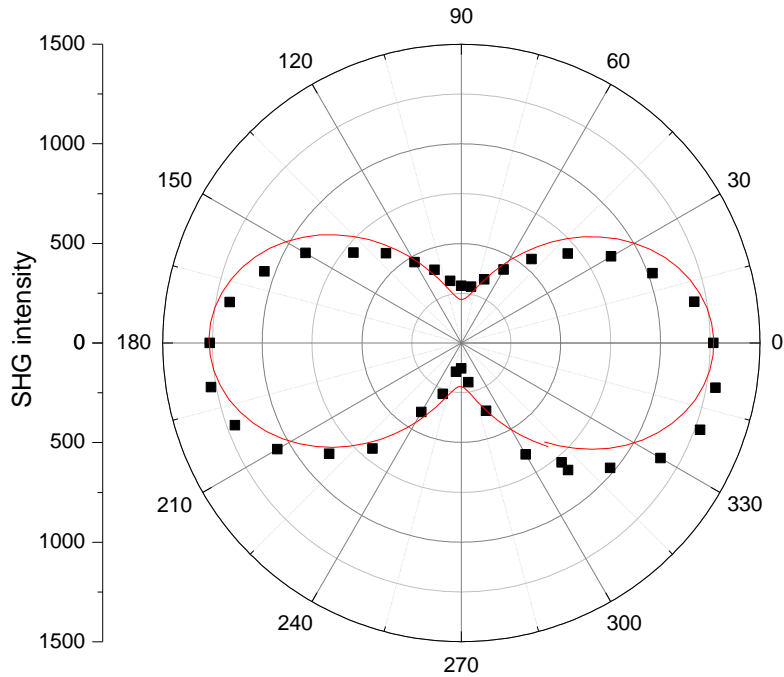


Fig. 4.1 SHG intensity is dependent on direction of polarization

Fig. 4.1 shows the relationship between SHG and direction of polarization, which is 0° or 180° when polarization is parallel to rubbing direction. In Fig. 4.1, there are two peaks and valleys. It shows SHG reaches maximum when polarization is parallel to the orientation of LC. Oppositely, while polarization is perpendicular to orientation, SHG intensity is lowest. According to 2.1.4, the two models of SHG in NLC are discussed, one is based on electric quadrupole moment, and the other one is due to the light-induced curvature strains. Considering electric quadrupole moment model, it should exhibit four peaks in the angle between director of NLC and direction of polarization. Therefore,

light-induced curvature strains model is more acceptable.



4.2 Switchable and repeatable SHG

When both 473-nm control light and 1030-nm excitation light are overlapped, SHG decreases significantly. First, 473-nm CW laser is used as control light. From Fig. 4.2, when the intensity of control light increases, the intensity of SHG decreases. In other words, SHG in DDLC is depleted by control light. The lowest SHG signal is not 0 but about 20%~30%. The possible reason is the PSF of excitation light is larger than the one of control light. In Fig. 4.3, red, green and blue curve mean normalized intensity distribution of excitation light, SHG and control light respectively. If we assume all SHG signal in the region of control light is suppressed, the remaining percentage of SHG signal could be expressed as

$$\left(1 - \frac{\int_0^{D_{control}} I_{SHG} r dr}{\int_0^{\infty} I_{SHG} r dr}\right) \times 100\% \cong 30\% \quad (4.1)$$

Where I_{SHG} means the intensity distribution of SHG, $D_{control}$ indicates the size of control light and r is radial position. The result, 30%, closely meets to our data

In addition, in Fig. 2.1, it seems SHG is easier to be suppressed by control light in thinner sample. Our explanation is, in thinner sample, confocal parameter is roughly equivalent to the thickness of sample. In contrast, confocal parameter is much smaller than the thickness of sample in thicker sample. It means there is some non-affected LC above and below the focus region in thicker sample but not in thinner one.

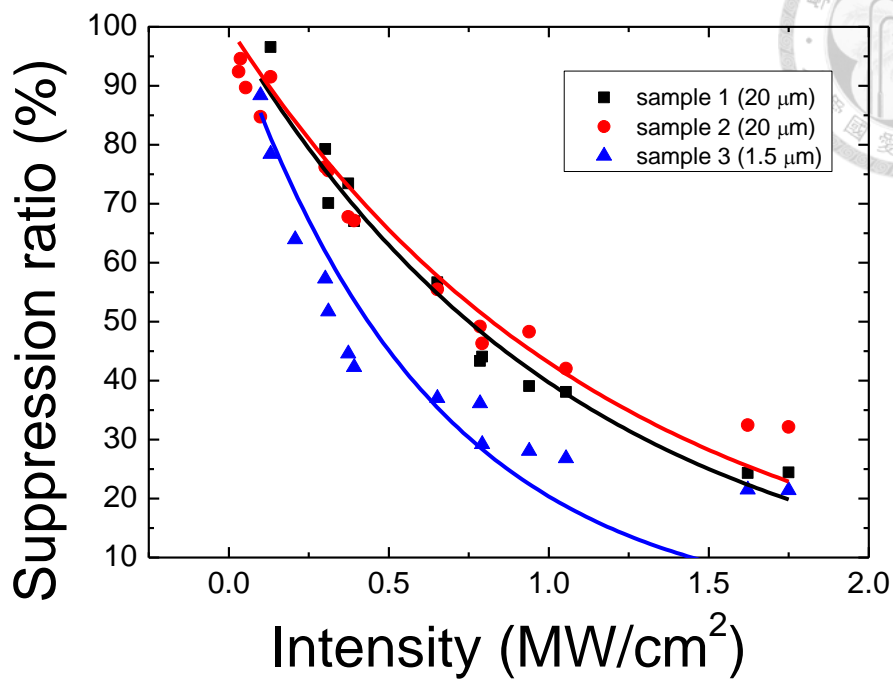


Fig. 4.2 SHG is depleted by control light, 473-nm CW laser

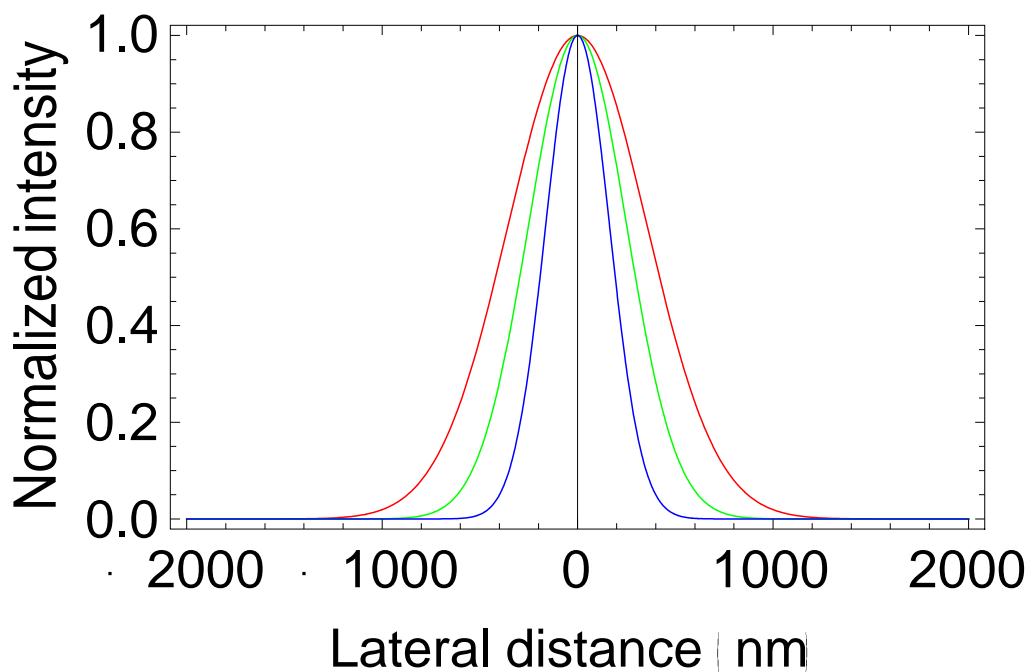


Fig. 4.3 Intensity distribution of PSFs in lateral direction. Red, green and blue curve mean normalized intensity distribution of excitation light, SHG and control light respectively.

On the other hand, in Fig. 4.4, if control light is turned on and off repeatedly, SHG signal does not decrease after several cycles. In other words, SHG signal shows the switchable and repeatable property.

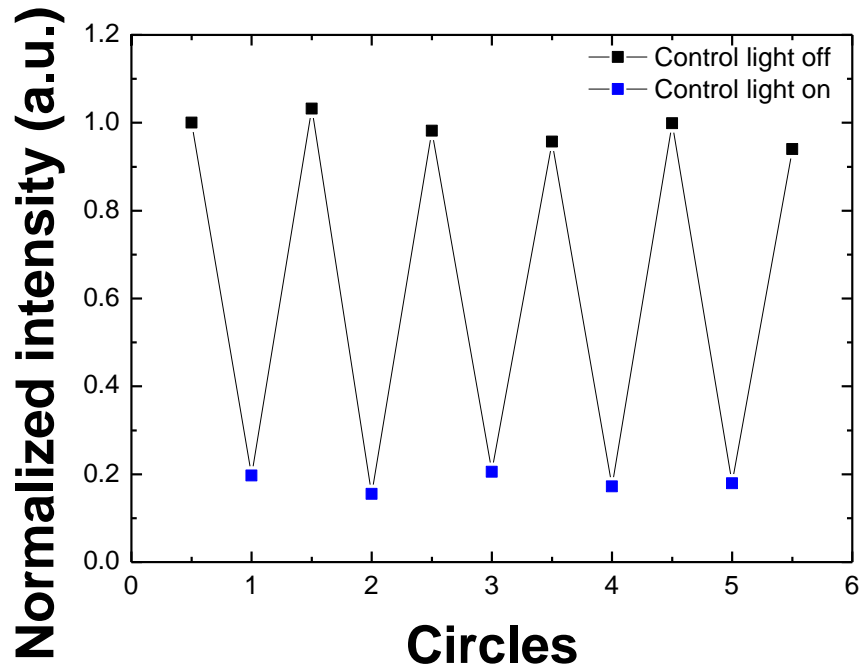
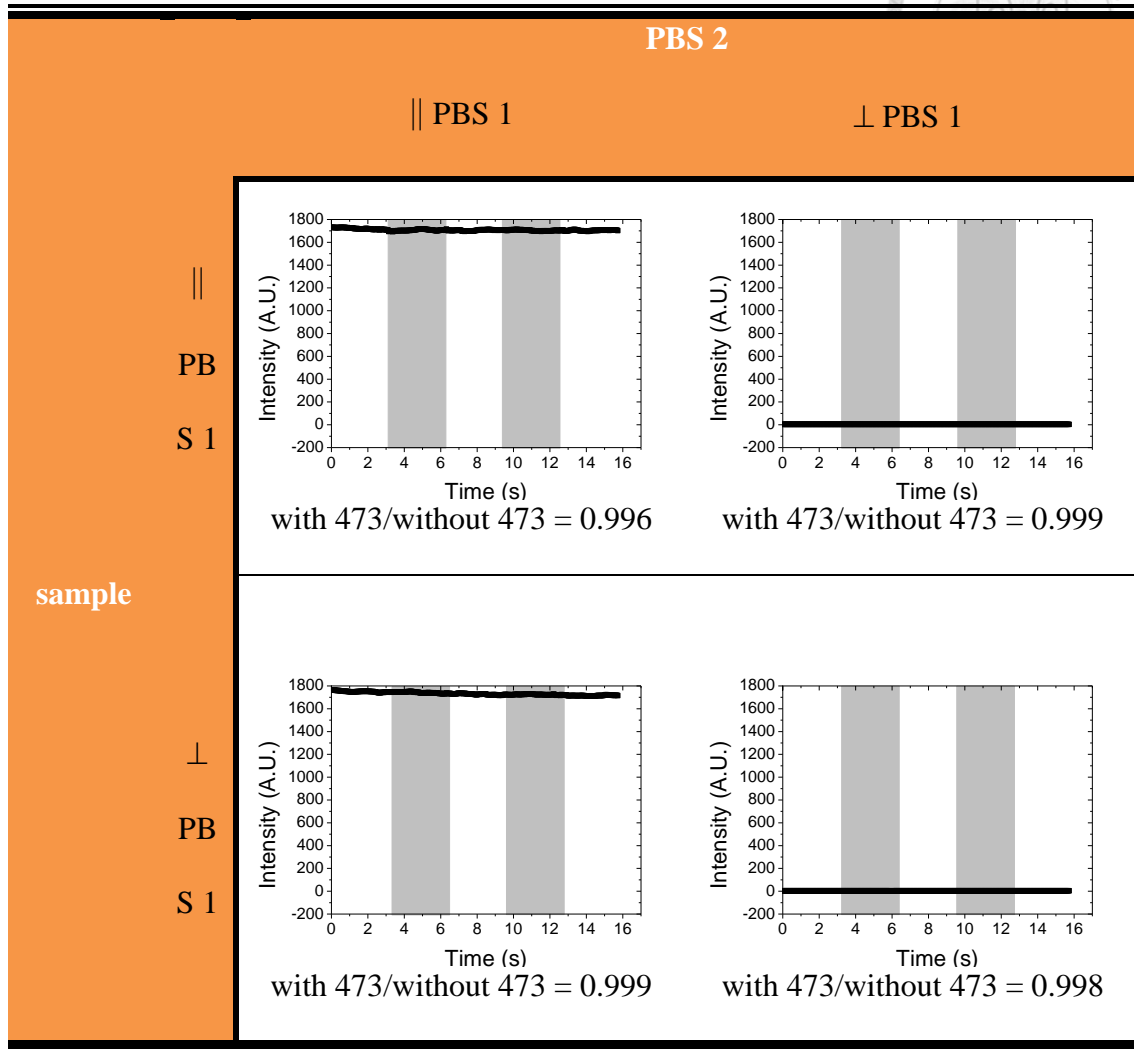
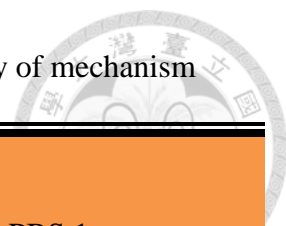


Fig. 4.4 Switchable and reversible optical controllable SHG

4.3 Mechanism of controllable SHG in DDLC

To determine the mechanism of DDLC is nematic-isotropic phase transition or optical Fredericks transition, polarized light microscope is used. Table 4.1 shows four results under different conditions described in 3.2. As shown in Fig. 3.4, the orientation of DDLC and direction of PBS 2 is parallel or perpendicular to PBS 1. From the results, it is obvious that the intensity of probe light is not altered by control light. It means the polarization of the probe light is not rotated. This result supports the hypothesis of phase transition.

Table 4.1 Result of polarized light microscope for the study of mechanism



4.4 Response time of phase transition

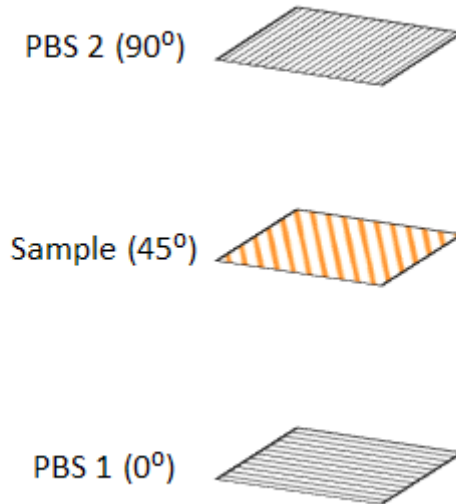


Fig. 4.5 The relationship between directions of two PBS and sample

To determine the response time of phase transition in DDLC, higher contrast is necessary. Therefore, we rotate sample and PBS 2 as shown in Fig. 4.5, resulting significant change of probe light transmittance when turning control light on (see Fig. 4.6). As shown in the inset of Fig. 4.6, response time is the interval between lowest (green line) to highest (blue line) intensity. Here, we define response time is the interval (yellow blocks) between 10% and 90% intensity change (two red lines). Obviously, the response time of nematic-to-isotropic is much faster than that of isotropic-to-nematic. The former one is about several tens of millisecond. Latter one is in second time scale. It is reasonable because nematic-to-isotropic phase change is due to liquid crystal heated by control light. In the other hand, isotropic-to-nematic phase transition is as a result of spontaneous cooling.

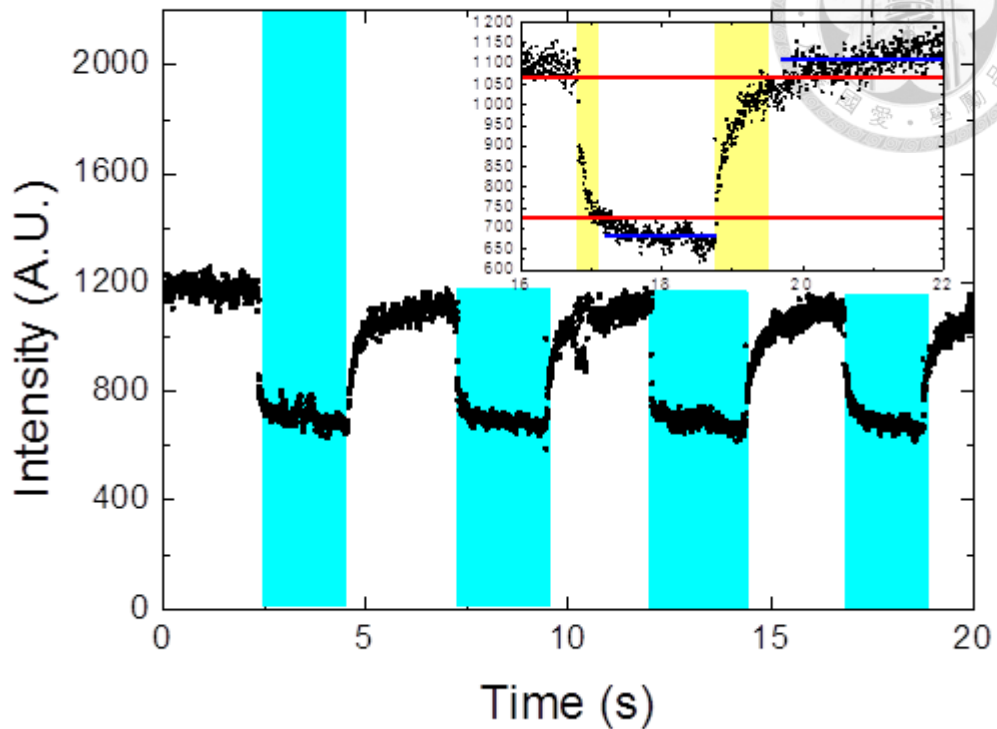


Fig. 4.6 Transmittance of probe light is changed by control light

4.5 Comparison with other optical controllable SHG

According to previous results of optical controllable SHG, the common drawbacks are low on-off contrast, limited switch circle and long response time. As mentioned before, the contrast is less than 50% while the response time is in hundreds of second scale. Some results which control SHG based on poled polymers suffer from irreversible changes after several on-off cycles. It causes SHG decay after illuminated by control light several times. From 4.2 and 4.4, it is obviously that all of these drawbacks are improved. The modulation depth, which means the percentage of SHG suppressed by control light, is 80%. Besides, the response time of nematic-to-isotropic and isotropic-to-nematic is in millisecond and second time scale respectively. Moreover, Fig. 4.4 shows SHG do not

decrease after several cycles.



4.6 RESOLFT-like SHG microscopy

Because our idea is origin from RESOLFT microscopy, it is acceptable to determine the resolution in same way presented in equation (2.34).

$$d_{theory} = d_c / \sqrt{1 + d_c^2 \cdot a^2 \cdot \frac{I_{control}}{I_{sat}}} \quad (4.2)$$

Where d_c means the FWHM of focal spot in a confocal microscope, a is the steepness factor, $I_{control}$ is the intensity of control light, I_{sat} saturation intensity, defined as the intensity of control light when half of the SHG depleted.

From Fig. 4.2, I_{sat} is about 1.5 MW/cm². Here, d_c is about 0.6 μm and a is about 3.7 μm⁻¹. Therefore, the theoretical resolution is about 280 nm when $I_{control}$ is 3.5 MW/cm². It's about two sevenths resolution of confocal microscopy, which is about 600 nm.

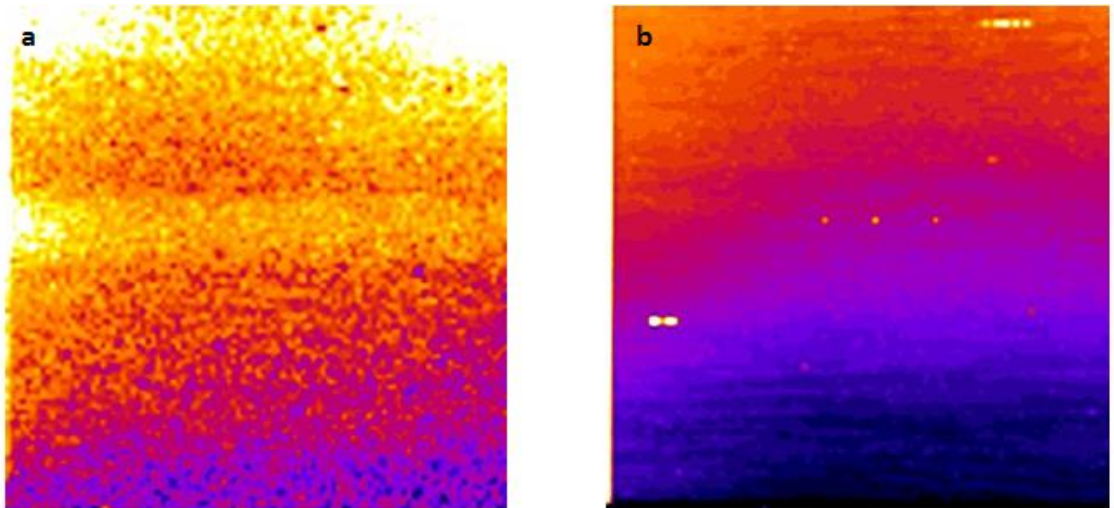


Fig. 4.7 SHG image of usual DDLC sample with (a) near-infrared laser only. (b) both near-infrared laser and doughnut-shaped control light. Both image sizes are

10 $\mu\text{m} \times 10 \mu\text{m}$.

However, due to lack of fine structure, it cannot determine improved resolution in usual DDLC sample, which is injected into two glasses coated with pre-aligned polymers as shown in Fig. 4.7. Therefore, some special treatments are needed.

4.6.1 Nano-gold-doped sample

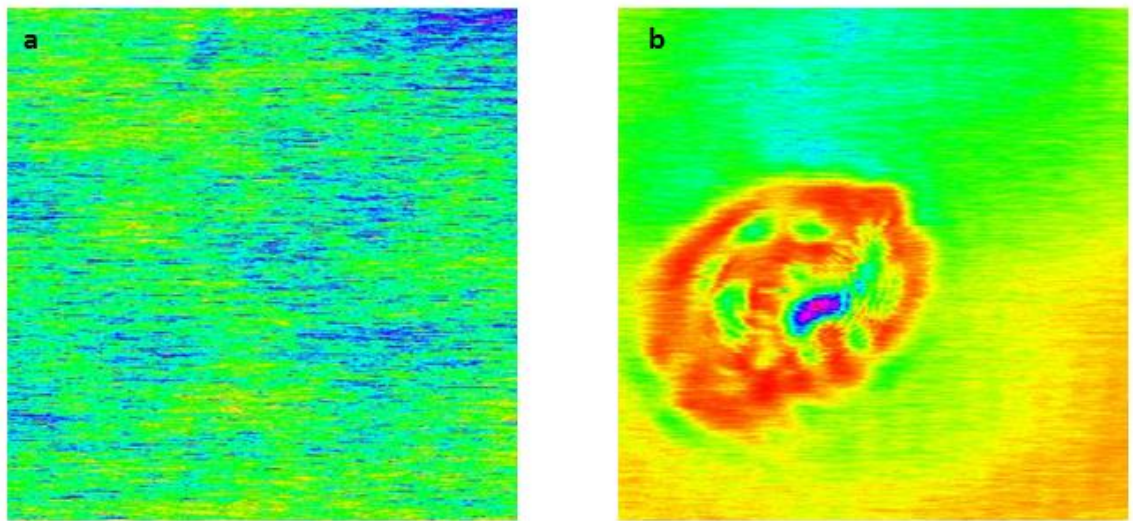
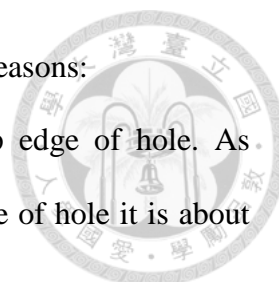


Fig. 4.8 Backward scattering image of nano-gold-doped DDLC sample (a) before (b) after illuminated by 473-nm laser. Both image sizes are 10 $\mu\text{m} \times 10 \mu\text{m}$.

Nevertheless, DDLC sample suffers from photodamage after illuminated by control light. As shown in Fig. 4.8, after intense control light turn on, strange pattern appear in SHG image. One of possible explanation is thermo effect induced by gold nanoparticle due to absorb 473-nm laser

4.6.2 Artificial structure made by photoresist

On the other hand, we also demonstrated SHG superresolution in artificial structure made by photoresist as mentioned in . However, we found it might



not be a good sample for demonstration due to following two reasons:

We expected to determine the resolution by the sharp edge of hole. As shown in Fig. 4.9, there is a strong SHG peak around the edge of hole it is about 1.3 μm (Fig. 4.9 (c)). It is too broad to determine the resolution.

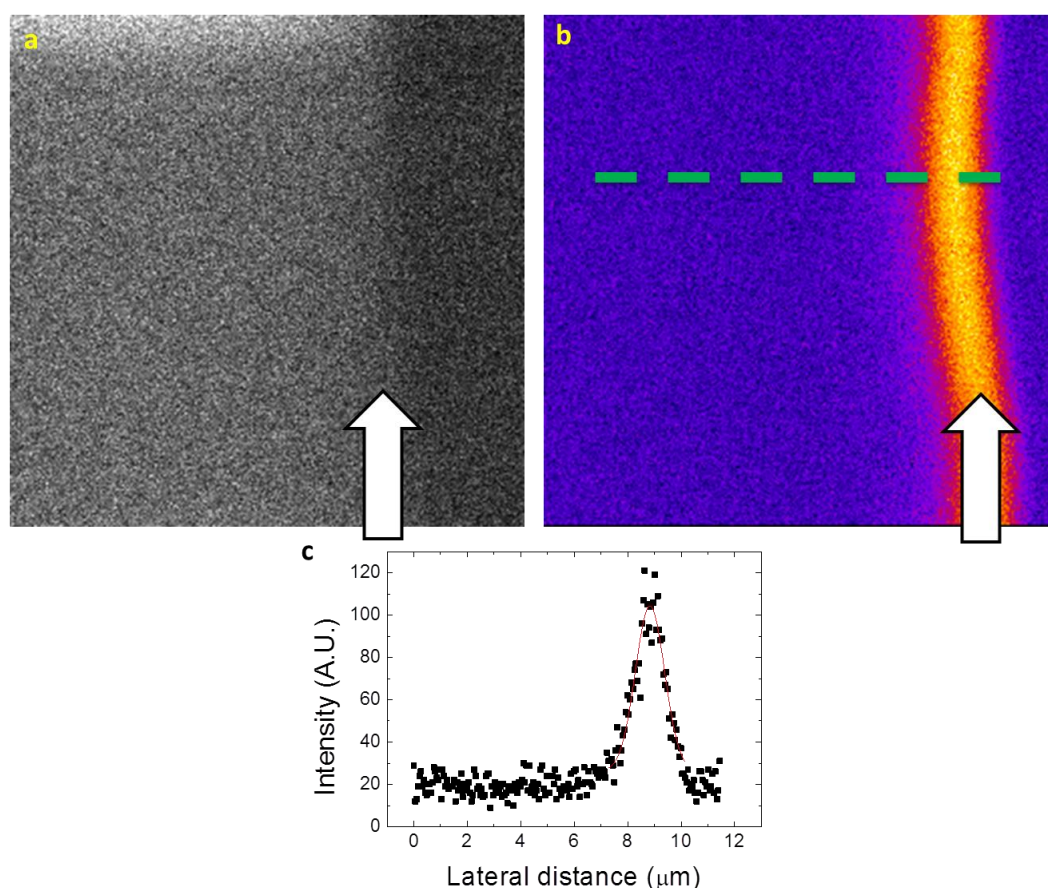


Fig. 4.9 (a) Backward scattering image and (b) SHG image of artificial structure.

Arrows point out the edge of hole. Both image sizes are $13.8 \mu\text{m} \times 13.8 \mu\text{m}$. (c)

Line profile of SHG image. The FWHM of the peak is about 1.3 μm , which is

much larger than the PSF. It means it could not be used to determine the

resolution.

Besides, photodamage also happened after sample illuminated by control light as shown in Fig. 4.10. It is because there is an UV absorption peak of photoresist. And the wavelength of control light we used is 473 nm, which is close

to UV.

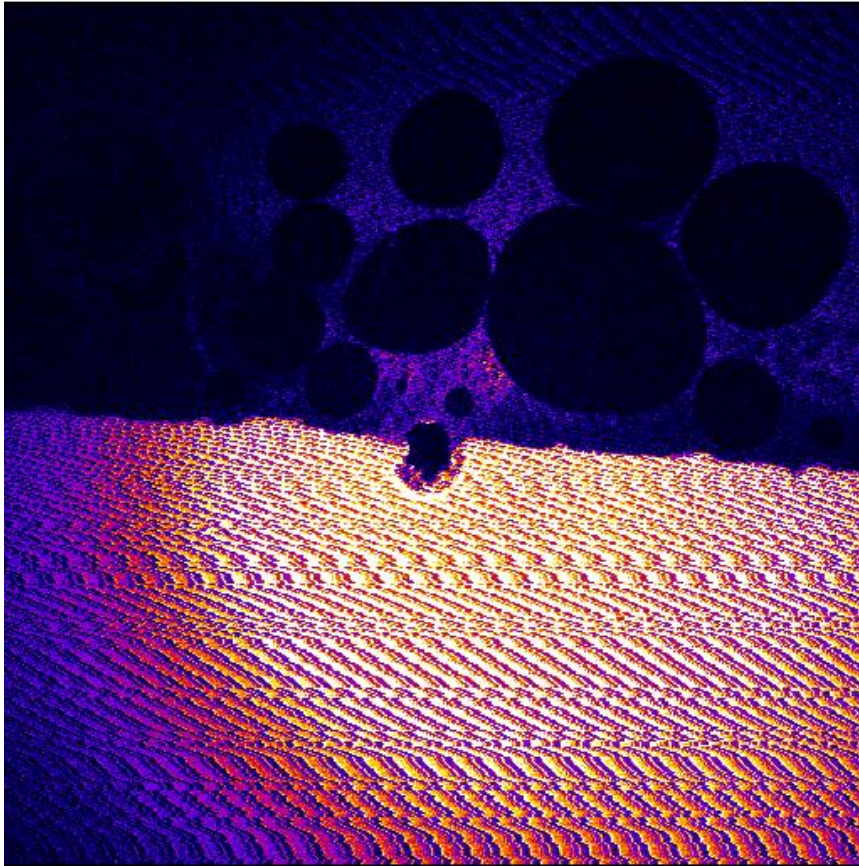


Fig. 4.10 Image of artificial structure after illuminated by control light. There is a obvious defect in the edge of hole due to photodamage. Image size is $360\ \mu\text{m} \times 360\ \mu\text{m}$.

Chapter 5 Conclusion

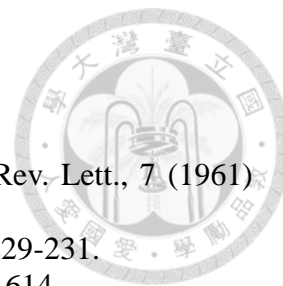


In the previous results of optically controllable second harmonic generation (SHG), they faced to several disadvantage, including long response time, low contrast and irreversible switch. In this thesis, we propose a novel way to demonstrate optically controllable second harmonic generation (SHG) based on dye-doped liquid crystal (DDLIC) to avoid these drawbacks. As a result, we demonstrated a reversible optically controllable SHG with 80%-modulation-depth and sub-second-scale-response-time.

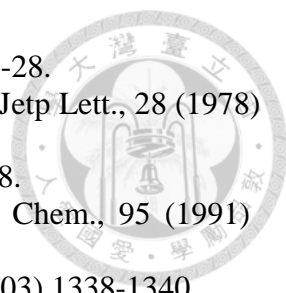
We also raise two possible mechanisms of our result. One is optical Fredericks transition. The other one is nematic-isotropic phase transition. After the test of transmittance, we claim our result is based on the nematic-isotropic phase transition. And a brief explanation about high-contrast, high-speed and reversible SHG switch is given.

In the final part of this thesis, similar to reversible saturable optical fluorescence transitions (RESOLFT) microscope, we point out this work have high potential to apply to bleaching-free superresolution microscope due to the capability of optically switch on/off. However, due to the limitation of samples, we could not get the resolution-enhanced result. And finding a more stable sample is a future work of this study.

REFERENCE



- [1] P. A. Franken, G. Weinreich, C. W. Peters, *et al.*, Phys. Rev. Lett., 7 (1961) 118-120.
- [2] W. Kaiser and C. G. B. Garrett, Phys. Rev. Lett., 7 (1961) 229-231.
- [3] S. Singh and L. T. Bradley, Phys. Rev. Lett., 12 (1964) 612-614.
- [4] R. W. Terhune, P. D. Maker and C. M. Savage, Phys. Rev. Lett., 8 (1962) 404-406.
- [5] T. H. Maiman, Nature, 187 (1960) 493-494.
- [6] W. R. Zipfel, R. M. Williams and W. W. Webb, Nat. Biotechnol., 21 (2003) 1368-1376.
- [7] R. D. Schaller, J. C. Johnson, K. R. Wilson, *et al.*, J. Phys. Chem. B, 106 (2002) 5143-5154.
- [8] D. Cotter, R. J. Manning, K. J. Blow, *et al.*, Science, 286 (1999) 1523-1528.
- [9] T. Brabec and F. Krausz, Rev. Mod. Phys., 72 (2000) 545-591.
- [10] R. L. Byer, IEEE J. Sel. Top. Quantum Electron., 6 (2000) 911-930.
- [11] K. B. Eisenthal, Chem. Rev., 96 (1996) 1343-1360.
- [12] K. Yoshino, M. Utsumi, Y. Morita, *et al.*, Liq. Cryst., 14 (1993) 1021-1032.
- [13] K. W. Chang, A. C. Chiang, T. C. Lin, *et al.*, Opt. Commun., 203 (2002) 163-168.
- [14] L. Boubekeur-Lecaque, B. J. Coe, K. Clays, *et al.*, J. Am. Chem. Soc., 130 (2008) 3286-3287.
- [15] R. Loucifsaibi, K. Nakatani, J. A. Delaire, *et al.*, Chem. Mat., 5 (1993) 229-236.
- [16] Y. Atassi, J. A. Delaire and K. Nakatani, J. Phys. Chem., 99 (1995) 16320-16326.
- [17] M. Sliwa, S. Letard, I. Malfant, *et al.*, Chem. Mat., 17 (2005) 4727-4735.
- [18] K. Nakatani and J. A. Delaire, Chem. Mat., 9 (1997) 2682-2684.
- [19] A. Priimagi, K. Ogawa, M. Virkki, *et al.*, Adv. Mater., 24 (2012) 6410-6415.
- [20] J. H. Lin, C. Y. Tseng, C. T. Lee, *et al.*, Opt. Express, 22 (2014) 2790-2797.
- [21] F. Castet, V. Rodriguez, J. L. Pozzo, *et al.*, Accounts Chem. Res., 46 (2013) 2656-2665.
- [22] C. Cojocariu and P. Rochon, Pure Appl. Chem., 76 (2004) 1479-1497.
- [23] A. A. Beharry and G. A. Woolley, Chem. Soc. Rev., 40 (2011) 4422-4437.
- [24] S. Xie, A. Natansohn and P. Rochon, Chem. Mat., 5 (1993) 403-411.
- [25] I. Janossy, A. D. Lloyd and B. S. Wherrett, Mol. Cryst. Liquid Cryst., 179 (1990) 1-12.
- [26] B. Saad, T. V. Galstyan, M. M. Denariez-Roberge, *et al.*, Opt. Commun., 151 (1998) 235-240.
- [27] I. Janossy, Phys. Rev. E, 49 (1994) 2957-2963.
- [28] T. Ikeda, J. Mater. Chem., 13 (2003) 2037-2057.
- [29] B. Huang, M. Bates and X. W. Zhuang, Annu. Rev. Biochem., 78 (2009) 993-1016.
- [30] S. W. Hell, Science, 316 (2007) 1153-1158.
- [31] S. W. Hell, Nat. Biotechnol., 21 (2003) 1347-1355.
- [32] P. Wang, M. N. Slipchenko, J. Mitchell, *et al.*, Nat. Photonics, 7 (2013) 450-454.
- [33] S. W. Chu, T. Y. Su, R. Oketani, *et al.*, Phys. Rev. Lett., 112 (2014).

- 
- [34] F. C. Frank, Discussions of the Faraday Society, (1958) 19-28.
- [35] S. M. Arakelyan, G. L. Grigoryan, S. T. Nersisyan, *et al.*, JETP Lett., 28 (1978) 186-189.
- [36] M. Copic and T. Ovsenik, Europhys. Lett., 24 (1993) 93-98.
- [37] F. Tournilhac, J. Simon, M. Barzoukas, *et al.*, J. Phys. Chem., 95 (1991) 7858-7862.
- [38] I. H. Chen, S. W. Chu, F. Bresson, *et al.*, Opt. Lett., 28 (2003) 1338-1340.
- [39] O. Y. Zhongcan and Y. Z. Zie, Phys. Rev. A, 32 (1985) 1189-1200.
- [40] D. M. Shotton, J. Cell Sci., 94 (1989) 175-206.
- [41] R. H. Webb, Rep. Prog. Phys., 59 (1996) 427-471.
- [42] Hellwart.R and Christen.P, Opt. Commun., 12 (1974) 318-322.
- [43] P. J. Campagnola and L. M. Loew, Nat. Biotechnol., 21 (2003) 1356-1360.
- [44] P. J. Campagnola, H. A. Clark, W. A. Mohler, *et al.*, J. Biomed. Opt., 6 (2001) 277-286.
- [45] M. J. Rust, M. Bates and X. W. Zhuang, Nat. Methods, 3 (2006) 793-795.
- [46] E. Betzig, G. H. Patterson, R. Sougrat, *et al.*, Science, 313 (2006) 1642-1645.
- [47] S. W. Hell, M. Dyba and S. Jakobs, Curr. Opin. Neurobiol., 14 (2004) 599-609.
- [48] K. I. Willig, S. O. Rizzoli, V. Westphal, *et al.*, Nature, 440 (2006) 935-939.
- [49] B. Harke, J. Keller, C. K. Ullal, *et al.*, Opt. Express, 16 (2008) 4154-4162.
- [50] V. Westphal and S. W. Hell, Phys. Rev. Lett., 94 (2005).
- [51] H. W. Kim, J. H. Mun, C. S. Yoon, *et al.*, Jpn. J. Appl. Phys. Part 2 - Lett., 40 (2001) 952-954.
- [52] G. A. R. Oliveira, E. R. A. Ferraz, F. M. D. Chequer, *et al.*, Mutat. Res. Genet. Toxicol. Environ. Mutagen., 703 (2010) 200-208.
- [53] G. Bachelier, J. Butet, I. Russier-Antoine, *et al.*, Phys. Rev. B, 82 (2010).
- [54] A. Capretti, E. F. Pecora, C. Forestiere, *et al.*, Phys. Rev. B, 89 (2014).